OUKA
The University of Osaka
Institutional Knowledge Archive

Title	Theory of Electromagnetism in Dipole Superfluids
Author(s)	山本, 和輝
Citation	大阪大学, 2026, 博士論文
Version Type	VoR
URL	https://doi.org/10.18910/105639
rights	
Note	

The University of Osaka Institutional Knowledge Archive : OUKA

https://ir.library.osaka-u.ac.jp/

The University of Osaka

Doctoral Thesis

Theory of Electromagnetism in Dipole Superfluids

Department of Physics, The University of Osaka

Kazuki Yamamoto

2026

Contents

List of publications **1**

1 Introduction **2**

1.1 Purpose of study 2

1.2 Magnon Bose-Einstein condensate 6

1.3 Aharonov-Casher phase 9

2 Theoretical background **11**

2.1 Geometric phases of monopoles and dipoles 11

2.1.1 Aharonov-Bohm phase 11

2.1.2 Aharonov-Casher phase 11

2.1.3 He-McKellar-Wilkens phase 13

2.2 Ginzburg-Landau theory of Superconductivity 14

3 Electric-field response in magnetic-dipole superfluids **17**

3.1 Pseudo-magnetic field by Aharonov-Casher effect 17

3.2 Positive feedback mechanism 18

3.3 Ginzburg-Landau theory 19

3.3.1 Formulation 19

3.3.2 Helmholtz free energy 21

3.3.3 Dimensionless equations 21

3.4 Single-vortex state 24

3.5 Vortex lattice 27

4 Magnetic-field response in electric-dipole superfluids **30**

4.1 Pseudo-magnetic field by He-McKellar-Wilkens effect 30

4.2 Negative feedback mechanism 31

4.3 Ginzburg-Landau theory . . . 32
4.3.1 Formulation . . . 32
4.3.2 Gibbs free energy . . . 33
4.3.3 Dimensionless equations . . . 33
4.4 Single-vortex state . . . 34
4.5 Vortex lattice . . . 35
4.6 Dipole superfluids and monopole superfluids . . . 35

5 Ferroelectric instability in magnetic-dipole superlfuids 38
5.1 Review: Bose-Hubbard model in conventional superfluids . . . 38
5.2 Bose-Hubbard model in magnetic-dipole superfluids . . . 40
5.3 Ferroelectricity . . . 42
5.4 Bosonic BdG Hamiltonian . . . 44
5.5 Bogoliubov-excitation spectrum . . . 45
5.6 Landau and dynamical instabilities . . . 47

6 Conclusion 48

A General properties of bosonic BdG Hamiltonian 50
A.1 Pseudo-Hemiticity . . . 51
A.2 Particle-hole symmetry . . . 52
A.3 Diagonalization by para-unitary matrix . . . 52
A.4 Two-band model . . . 53

B Thermodynamic free energy 55
B.1 Magnetic-dipole superfluids . . . 55
B.2 Electric-dipole superfluids . . . 56

Acknowledgments 58

Bibliography 58

List of publications

- Paper I

  Topological gap labeling with third Chern numbers in three-dimensional quasicrystals

  Kazuki Yamamoto and Mikito Koshino

  Physical Review B **105**, 115410 (2022)

- Paper II

  Electromagnetic response in dipole superfluids

  Kazuki Yamamoto, Takuto Kawakami and Mikito Koshino

  Communications Physics **8**, 171 (2025)

- Paper III

  Time-reversal invariant vortex in topological superconductors and gravitational $\mathbb{Z}_2$ topology

  Kazuki Yamamoto, Naoto Kan and Hidenori Fukaya

  arXiv number: 2507.06586 (2025)

  Accepted in Physical Review B

- Paper IV

  Ferroelectricity in magnon Bose-Einstein condensate: non-reciprocal superfluidity, exceptional points and Majorana bosons

  Kazuki Yamamoto, Takuto Kawakami, Mikito Koshino

  arXiv number: 2512.22073 (2025)

The present thesis is based on Papers II and IV.

Chapter 1

Introduction

1.1 Purpose of study

When a magnetic field is applied to a superconductor, an electric supercurrent flows to expel the external magnetic field, a phenomenon known as the Meissner effect. This arises from a unique interaction between the condensate of charged particles and the electromagnetic field. However, condensates can also form from particles with different electromagnetic properties. Of particular interest is a superfluid composed of charge-neutral particles that possess a magnetic dipole moment. Recent attention has focused on such systems, including spin-triplet excitonic insulators [1–10] and magnon Bose-Einstein condensates (BECs) [11–27].

In general, magnetic dipoles experience a geometrical phase known as the Aharonov-Casher (AC) phase [28], analogous to the Aharonov-Bohm (AB) phase observed for charged particles in magnetic fields. In the AC effect, an electric field acts as an effective vector potential, and hence spatial variations in the electric field generate a pseudo-magnetic field [29–33], which plays a role analogous to the real magnetic field in the AB effect. The AC effect has been observed in a wide range of systems, including neutrons [34], atomic systems [35], mesoscopic systems [36–41], Josephson vortices [42–44], and spin waves [45, 46]. In particular, the AC effect serves as a fundamental basis for spin-current-driven electric polarization, enabling multiferroicity in magnetic materials. [47–56]

This raises a natural question: When magnetic dipoles condense into a superfluid, how do they respond to a pseudo-magnetic field (a spatially varying electric field) induced by the AC effect? The interaction between magnetic-dipole superfluids and the AC phase has been explored from various theoretical perspectives [57–62]. In this work, we propose a Ginzburg-Landau phenomeno-

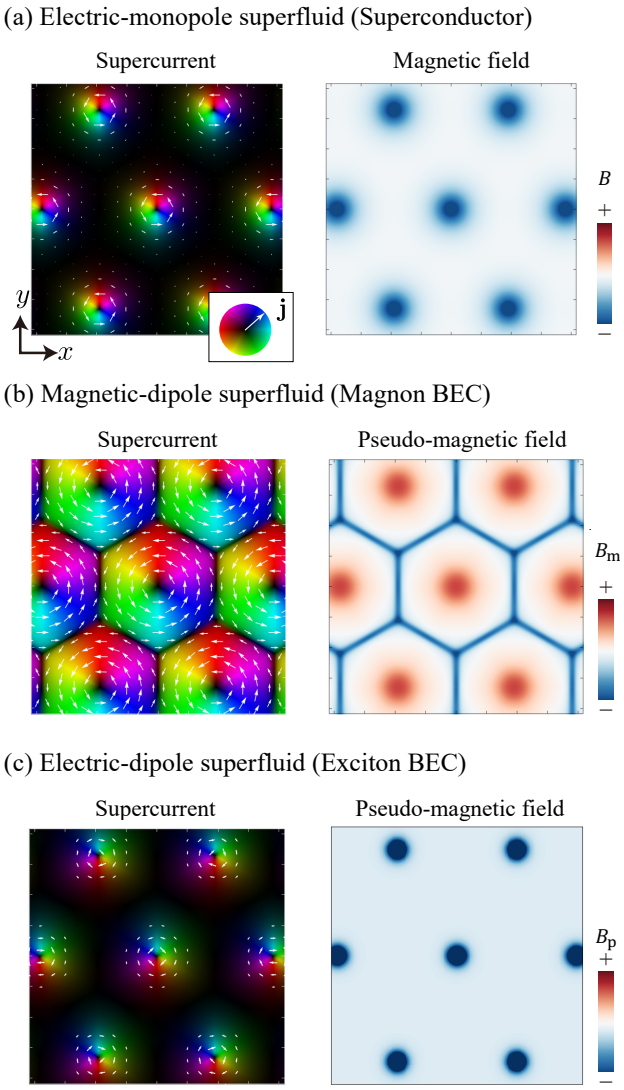


Figure 1.1: **Vortex lattices of monopole and dipole superfluids.** (a) a type-II superconductor (electric-monopole superfluid) under a magnetic field, (b) a magnetic-dipole superfluid under a pseudo-magnetic field, and (c) an electric-dipole superfluid under a pseudo-magnetic field. In all cases, we apply an external (pseudo) magnetic field in the negative z direction. The left panel plots the monopole supercurrent (not including negative charge) in (a), the magnetic-dipole supercurrent in (b), and the electric-dipole supercurrent in (c) with arrows and colors indicating the magnitude and direction. The right panel depicts the distribution of the real magnetic field in (a), and the pseudo-magnetic field in (b)and (c).

logical theory to describe dipole superfluids in external electromagnetic fields, revealing behavior that starkly contrasts with that of superconductors. We find that, under a pseudo-magnetic field, a dipole superfluid spontaneously forms a vortex lattice similar to a type-II superconductor, though the field texture is nearly the inverse of what is observed in conventional type-II superconductors. Figure 1.1 compares the vortex lattices in (a) a type-II superconductor (electric-monopole superfluid) under a magnetic field and (b) a magnetic-dipole superfluid under a pseudo-magnetic field, which constitutes the main result of this work. In each figure, the left panel illustrates the distribution of the supercurrent, and the right panel depicts the distribution of the real magnetic field in (a) and the pseudo-magnetic field in (b). In the superconductor [Fig. 1.1(a)], the supercurrent circulates only in the vicinity of the vortices, where the magnetic field is concentrated. In contrast, in the magnetic-dipole superfluid, the circulation of the supercurrent extends to the hexagonal boundaries separating the vortices, where the supercurrent abruptly changes direction and pseudo-magnetic field is sharply localized. These boundaries are singular planes for physical variables: supercurrent, electric polarization, order parameter derivatives are discontinuous, and pseudo-magnetic field and electric charge density diverge. The formation of these singular walls occurs abruptly when the coupling strength between the dipole superfluid and the electromagnetic field exceeds a specific critical value.

Additionally, we also investigate superfluids of *electric* dipoles, where electric and magnetic roles are reversed. Representative physical systems are exciton BECs [63–78], where excitons are charge-neutral and possess an electric-dipole moment. When a magnetic field is applied to the electric-dipole, it experiences an geometric phase, called He-McKellar-Wilkens (HMW) phase [79, 80], that is the electric-dipole counterpart of AC phase in the magnetic-dipoles. We formulate the Ginzburg-Landau theory and obtain vortex lattices in an analogous way to the case of magnetic-dipole superfluids. Interestingly, we find that the behaviors are significantly different from those in magnetic-dipole superluids, where the supercurrent and the pseudo-magnetic field is concentrated only at vortex cores as illustrated in Fig. 1.1(c), resembling the behavior observed in superconductors.

Furthermore, we revealed that the contrasting behaviors of magnon and electronic systems originate from the opposite signs of the electromagnetic feedback generated by their orbital motion. In conventional electronic systems, orbital motion driven by an external magnetic field induces a magnetization that screens the applied field, thereby exhibiting negative feedback. In sharp contrast, in magnon systems, orbital motion driven by an external electric field induces an electric polarization

that reinforces the applied field, leading to positive feedback. Thus, the orbital magnetization and orbital polarization exhibit mutually inverted responses with respect to magnetic and electric fields. Interestingly, this relation is not a peculiar feature of the present system but is also familiar from ordinary paramagnets and paraelectrics. Indeed, while paramagnets develop magnetization that strengthens the magnetic field, paraelectrics develop polarization that weakens the electric field. Hence, the sign reversal of electromagnetic feedback between electric and magnetic fields reflects a general and fundamental property rooted in basic electrodynamics.

Such a positive feedback effect of the electric field in magnon systems suggests the possibility of electric polarization emerging even in the absence of an external electric field, i.e., a ferroelectric transition. Motivated by the above, we investigate a ferroelectric instability of a magnon Bose–Einstein condensate, mediated by its interaction with an electric field through a geometric Aharonov–Casher (AC) phase. A distinct feature of the system is the positive feedback loop in which an electric field induces magnon orbital motion via the AC phase, generating electric polarization that in turn enhances the original field. Based on bosonic Bogoliubov–de Gennes (BdG) mean-field theory, we show that this feedback drives a spontaneous ferroelectric transition in the magnon superfluid, accompanied by a persistent magnon supercurrent. In the resulting ferroelectric phase, the quasiparticle excitation spectrum becomes nonreciprocal, reflecting spontaneous breaking of spatial inversion symmetry. At the critical point of the transition, the bosonic BdG Hamiltonian exhibits coalescence of both eigenvalues and eigenvectors, forming an exceptional point. The corresponding eigenvector is an equally weighted superposition of bosonic quasiparticle and quasihole states and is invariant under particle–hole transformation, allowing it to be interpreted as a bosonic analog of a Majorana fermion.

The thesis is organized as follows. In the rest of this chapter, we review the basics of the magnon BEC and the AC phase. In Chapter 2, we review the theoretical background. In Chapter 3, we find the positive feedback effect inherent to magnon BEC, formulate the phenomenological theory and study their vortex states under pseudo-magnetic field. In Chapter 4, we study its electromagnetic duals, namely electric-dipole superfluids. In Chapter 5, we propose the microscopic theory of magnon BEC and reveal the ferroelectricity driven by the positive feedback effect. In Chapter 6, we describe conclusion and outlook.

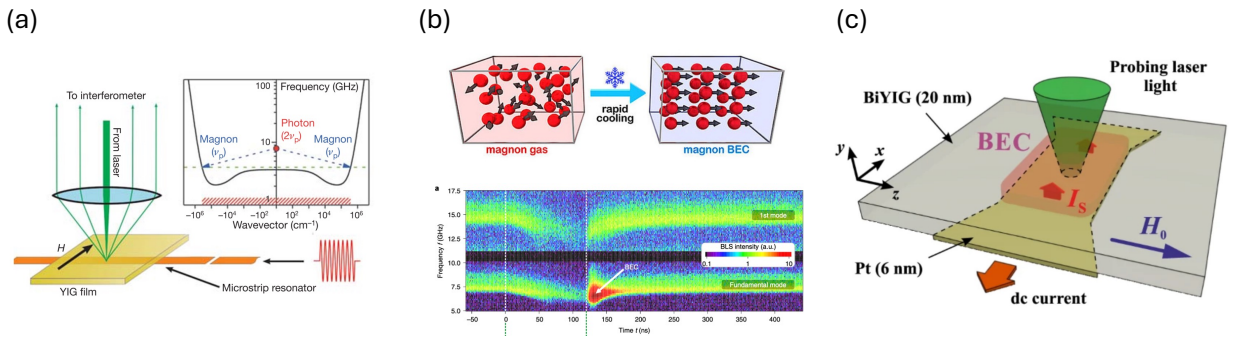


Figure 1.2: **Experimental technique to observe magnon BEC in YIG.** The formation of a magnon BEC requires the injection of nonequilibrium magnons through incoherent driving, such as (a) parametric pumping [11, 12, 81], (b) rapid cooling of the thermal magnons [82] and (c) spin-transfer torque [15].

1.2 Magnon Bose-Einstein condensate

Here, we review the concept of the magnon BEC and its experimental realizations, since it is an representative physical system of magnetic-dipoles superfluids, which is the main focus of this doctoral thesis.

Magnon

Magnons are bosonic quasiparticles that represent quantized collective excitations of spins in magnetically ordered systems. From a fundamental viewpoint, they emerge as low-energy degrees of freedom associated with the spontaneous breaking of continuous spin-rotational symmetry, and can be understood as the quantum counterparts of classical spin waves. As such, magnons play a role analogous to phonons in crystals, providing a universal description of collective dynamics in magnetic insulators.

Magnons also serve as fundamental carriers of spin angular momentum and energy in insulating magnets. Since magnons carry a quantized magnetic dipole moment but no electric charge, they enable the transport of spin and energy without accompanying charge currents. This gives rise to purely bosonic quantum transport phenomena, such as magnon spin currents and magnon heat currents, which are free from Joule heating and dissipation mechanisms intrinsic to electronic transport. Moreover, magnons exhibit quantum characteristics, including the ability to undergo Bose–Einstein condensation (BEC).

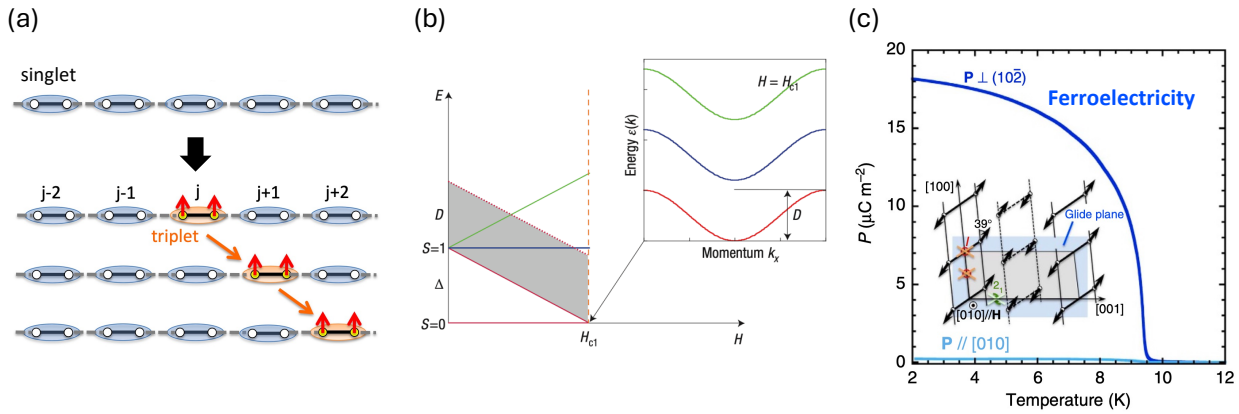


Figure 1.3: **Magnon BEC in quantum dimer magnet $TlCuCl_3$.** (a) Schematic figures of quantum spin dimer system with singlet and triplet states. [24] (b) Behaviors of magnon (triplon) band dispersions with increasing external magnetic field. [18] (c) Experimentally observed temperature dependence of electric polarization **P** in magnon BEC, signaling ferroelectricity. [24]

Magnon BEC in Yttrium Iron Garnet (YIG)

The magnon Bose-Einstein condensate (BEC) at room temperature is a remarkable phenomenon that was first observed in 2006 [11], in high-quality yttrium iron garnet (YIG)—an easy-plane ferrimagnetic insulator characterized by exceptionally low magnetic dissipation. The formation of a magnon condensate requires the injection of nonequilibrium magnons through incoherent driving mechanisms, such as parametric pumping [11, 12, 81], rapid cooling of the thermal magnons [82], or spin-transfer torque [15]. When the nonequilibrium magnon density exceeds a critical threshold, the magnons undergo (quasi)thermalization and accumulate at the band minimum, resulting in the formation of a quasi-equilibrium magnon condensate. Furthermore, the temperature gradient driven magnon supercurrent is also demonstrated experimentally in this system. [15] The Josephson oscillation of the magnon BEC is also presented experimentally [83].

Magnon BEC in quantum dimer magnet

Another important physical platform for realizing magnon Bose–Einstein condensation (BEC) is quantum spin-dimer systems [18], represented by $TlCuCl_3$, in which nearest neighbor copper ions Cu^{2+} carrying $S = 1/2$ are coupled via antiferromagenetic exchange interactions, and the intradimer coupling is much stronger than the interdimer coupling. As a result, the ground state is well approximated by a direct product of spin-singlet states on each dimer bond, since the energy of the singlet ($S = 0$) is lower than the triplet ($S = 1$). The system therefore remains a quantum paramagnet down to the lowest temperatures. See Fig. 1.3 (a).

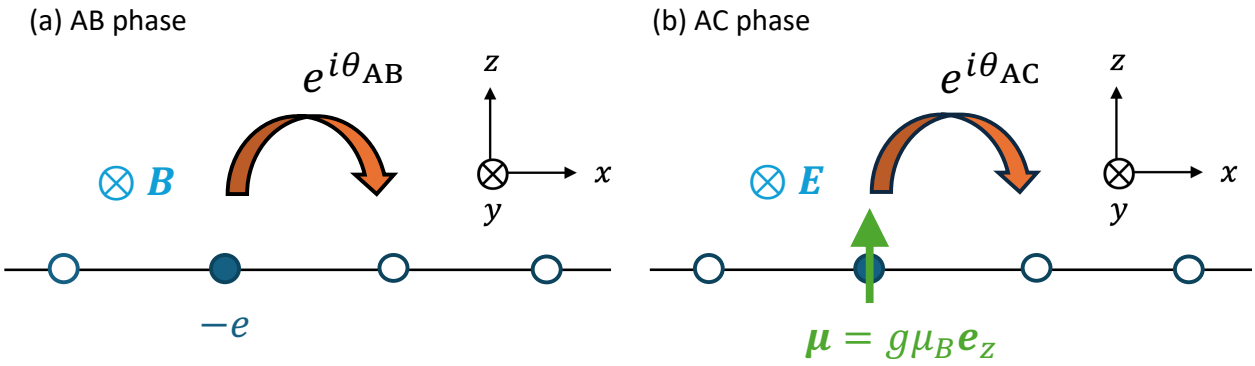


Figure 1.4: **Schematic figures of AB and AC phase.** (a) Electrons under magnetic field experiences the AB phase and (b) magnons under electric fields experiences the AC phase.

The elementary excitations are triplet states on a dimer, which can propagate through the lattice via interdimer weak exchange interactions. These propagating triplets can be regarded as bosonic quasiparticles carrying a quantized magnetic dipole moment, known as triplons. Triplons can be viewed as magnetic quasiparticles analogous to magnons in ordered magnets obtained from the Holstein–Primakoff transformation. Since both excitations share the same quantum numbers, the two terms are sometimes used interchangeably. Owing to the interdimer coupling, the magnon or triplon excitations acquire a finite dispersion.

When an external magnetic field **H** is applied, as shown in Fig. 1.3 (b), the Zeeman coupling lifts the threefold degeneracy of the triplet excitations, splitting the magnon band into three branches labeled by the magnetic quantum number $S_z = -1, 0, +1$ where the z-axis is defined along the field direction. In Fig. 1.3 (b), three branches are labeled by the green, blue and red dispersions. With increasing field strength, the $S_z = +1$ branch is shifted downward in energy and eventually approaches the singlet ground state. At a critical field, the excitation gap closes, signaling the onset of magnon Bose–Einstein condensation. [18]

Ferroelectricity in magnon BEC

This magnetic-field-induced magnon BEC has been experimentally observed in the magnetic insulator $TlCuCl_3$, which subsequently stimulated extensive theoretical and experimental studies aimed at uncovering novel quantum phenomena. [18] In particular, in 2016, Kimura et al. [24] experimentally demonstrated ferroelectricity induced by magnon Bose–Einstein condensation through measurements of the dielectric constant and pyroelectric current. Fig. 1.3 (c) illustrates the temperature dependence of the electric polarization, showing ferroelectricity in magnon BEC. More

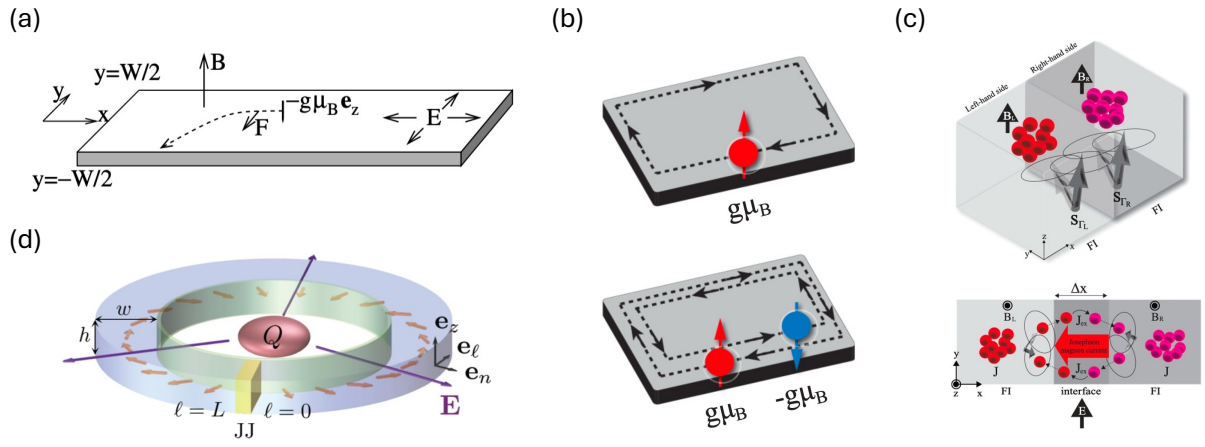


Figure 1.5: **Previous works on magnons with AC phase.** Several previous works about magnonic systems utilize the analogy to the electronic systems, such as (a) magnonic Lorentz force [29], (b) magnonic quantum Hall and quantum spin Hall insulators [30], (c) Josephson effect for magnon BEC [57] and (d) magnonic superfluid quantum interference device (SQUID) [54].

recently, detailed experimental studies have reported ferroelectricity in magnon BEC in a variety of quantum spin systems, including $Rb_2Cu_2Mo_3O_{12}$ [84] and $Cs_2Cu_2Mo_3O_{12}$ [85].

1.3 Aharonov-Casher phase

Geometric phases are a fundamental concept in modern condensed matter physics. A classic example is the Aharonov–Bohm (AB) phase, which arises in electronic systems subjected to a magnetic field. This idea can be extended by considering the geometric phases for a magnetic dipole in an electric field, that is known as the Aharonov-Casher (AC) phase [28]. When a magnetic dipole moment $\boldsymbol{\mu} = \mu \mathbf{e}_z$ moves in an electric field $\mathbf{E}$, it acquires the AC phase [28],

$$\theta_{\mathrm{AC}} = -\frac{1}{\hbar}\int \mathbf{A}_{\mathrm{m}} \cdot d\mathbf{r}, \tag{1.1}$$

where an effective vector potential is defined by

$$\mathbf{A}_{\mathrm{m}} = g_{\mathrm{AC}} \mathbf{E} \times \mathbf{e}_z \tag{1.2}$$

The constant $g_{\mathrm{AC}}(> 0)$ represents the strength of the spin-orbit coupling, and depends on the detail of the material. In vacuum, the g_{AC} is μ/c^2, where c is the speed of light. For magnons in a typical magnetic insulator, g_{AC} greatly enhances and is typically 10^6 times as large as in vacuum [47, 48].

Pseudo-magnetic field

Being perpendicular to $\mathbf{e}_z$, $\mathbf{A}_\mathrm{m}$ becomes a two dimensional vector with A^x_m and A^y_m components. The corresponding pseudo-magnetic field along z-direction is then written as

$$B_\mathrm{m} = (\boldsymbol{\nabla} \times \mathbf{A}_\mathrm{m})_z = -g_\mathrm{AC}\left(\frac{\partial E^x}{\partial x} + \frac{\partial E^y}{\partial y}\right). \tag{1.3}$$

Unlike the usual vector potential in AB phase, the effective vector potential $\mathbf{A}_\mathrm{m}$ does not have a gauge degrees of freedom, since it is directly expressed by the electric field. In this context, an electric field acts as an effective vector potential for magnons, and the spatially varying electric field gives rise to a pseudo-magnetic field. [29–31, 33, 46, 86–98] Consequently, several studies have proposed that such an effective vector potential can give rise to physical phenomena analogous to those observed for electrons in magnetic fields, including the Hall effect and the formation of Landau levels. [29, 31] The magnonic analog of quantum Hall and quantum spin Hall insulators has also been proposed. [30] The effect of AC phase on magnon BEC is also studied theoretically, including magnonic Josephson junction [57] and magnonic superfluid quantum interference devices (SQUID) [54], where the magnon supercurrent is controlled via the AC phase.

Electric polarization by magnon orbital motion

Another important aspect of the AC phase is its reciprocal phenomenon; the magnon orbital motion induces electric polarization, giving

$$\mathbf{P} = g_\mathrm{AC}\mathbf{j}_\mathrm{m} \times \mathbf{e}_z, \tag{1.4}$$

where $\mathbf{P}$ is the electric polarization and $\mathbf{j}_\mathrm{m}$ is the magnon current density. This mechanism was first demonstrated microscopically by Katsura et al. [47]. In the spin-system framework, a non-collinear spin texture is naturally interpreted as a spin current, leading to the emergence of electric polarization. It serves as a fundamental basis for spin-current-driven electric polarization, enabling multiferroicity in magnetic materials. [47–56]

Chapter 2

Theoretical background

2.1 Geometric phases of monopoles and dipoles

2.1.1 Aharonov-Bohm phase

Geometric phases are a fundamental concept in modern condensed matter physics. A classic example is the Aharonov–Bohm (AB) phase, which arises in electronic systems subjected to a magnetic field, giving

$$\theta_{\mathrm{AB}} = -\frac{e}{\hbar}\int \mathbf{A}\cdot d\mathbf{r}, \tag{2.1}$$

where $-e$ is the charge of an electron and $\mathbf{A}$ is the vector potential. This originates from the minimal coupling between electrons and the magnetic field, which is represented by the Lagrangian

$$L = \frac{1}{2}m_e\mathbf{v}^2 - e\mathbf{v}\cdot\mathbf{A}, \tag{2.2}$$

where m_e is a mass of an electron and $\mathbf{v}$ is the velocity of the electron.

This idea can be extended by considering the geometric phases for a magnetic/electric dipole in an electric/magnetic field, that is known as the Aharonov-Casher (AC) phase [28]/He-McKellar-Wilkens (HMW) phase [79, 80], respectively.

2.1.2 Aharonov-Casher phase

When a magnetic dipole moment $\boldsymbol{\mu} = \mu\mathbf{e}_z$ moves in an electric field $\mathbf{E}$, it acquires the Aharonov-Casher (AC) phase [28],

$$\theta_{\mathrm{AC}} = -\frac{1}{\hbar}\int \mathbf{A}_{\mathrm{m}}\cdot d\mathbf{r}, \tag{2.3}$$

where an effective vector potential is defined by

$$\mathbf{A}_{\rm m} = g_{\rm AC}\mathbf{E} \times \mathbf{e}_z \tag{2.4}$$

The constant $g_{\rm AC}(> 0)$ represents the strength of the spin-orbit coupling, and depends on the detail of the material. In vacuum, the $g_{\rm AC}$ is μ/c^2, where c is the speed of light. For magnons in a typical magnetic insulator, $g_{\rm AC}$ greatly enhances and is typically 10^6 times as large as in vacuum [47, 48].

We present a simplified derivation of the original Aharonov-Casher (AC) phase [28] in vacuum as a relativistic effect. We consider a particle with a magnetic-dipole $\boldsymbol{\mu} = \mu\,\mathbf{e}_z$, which is moving with velocity $\mathbf{v}$. The magnetic-dipole is equivalent to a small loop electric current on the xy-plane. When the loop current moves with velocity $\mathbf{v}$ relative to the rest frame, we (an observer in the rest frame) observe electric charge density $\rho = \mathbf{v}\cdot\mathbf{j}/c^2$ from Lorentz covariance. Here $\mathbf{j}$ is the current density in the moving frame fixed to the loop current. When a square loop current is moving along the x-axis, therefore, two sides along x are positively and negatively charged as illustrated in Fig. 2.1(a), resulting in an electric dipole

$$\mathbf{p} = g_{\rm AC}\mathbf{v} \times \mathbf{e}_{\rm z}, \tag{2.5}$$

where $g_{\rm AC} = \mu/c^2$.

If an external electric field $\mathbf{E}$ is present, the particle has an electrostatic potential energy $-\mathbf{p}\cdot\mathbf{E}$. Thus, the Lagrangian for the particle is given by

$$L = \frac{1}{2}m^*\mathbf{v}^2 + \mathbf{p}\cdot\mathbf{E}, \tag{2.6}$$

where m^* is a mass of the particle. As the second term is transformed as $\mathbf{p}\cdot\mathbf{E} = g_{\rm AC}(\mathbf{v}\times\mathbf{e}_{\rm z})\cdot\mathbf{E} = -g_{\rm AC}(\mathbf{E}\times\mathbf{e}_{\rm z})\cdot\mathbf{v}$, the Lagrangian is written as

$$L = \frac{1}{2}m^*\mathbf{v}^2 - \mathbf{v}\cdot\mathbf{A}_{\rm m}, \tag{2.7}$$

where $\mathbf{A}_{\rm m} = g_{\rm AC}\mathbf{E}\times\mathbf{e}_{\rm z}$. Since Eq. (2.7) is formally equivalent to the Lagrangian of an electron in a magnetic field, $\mathbf{A}_{\rm m}$ plays the role of the effective vector potential for the magnetic-dipole. Therefore, the moving magnetic-dipole acquires the AC phase [Eq. (3.1)].

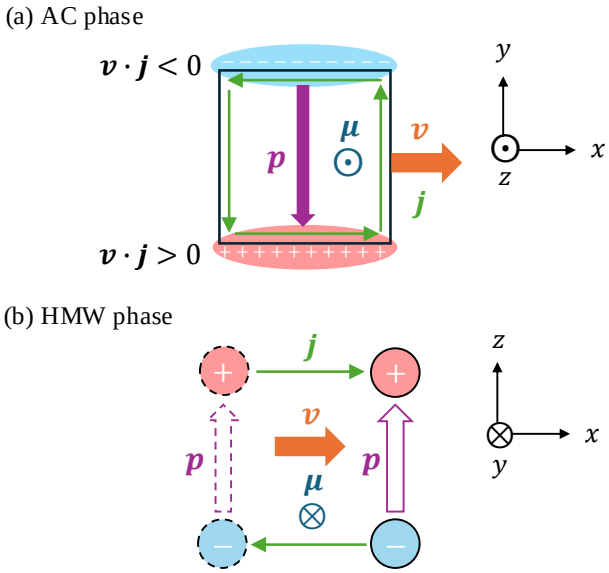


Figure 2.1: **Electric/magnetic dipole induced by the motion of magnetic/electric dipole.** Schematic figure for (a) a moving magnetic-dipole (loop current) with induced electric dipole, and (b) a moving electric-dipole with induced magnetic-dipole.

2.1.3 He-McKellar-Wilkens phase

The electric dipole $\mathbf{p} = p\mathbf{e}_z$ interacts with the magnetic flux density $\mathbf{B}$ by means of the He-McKellar-Wilkens (HMW) phase [77–80, 99–103],

$$\theta_{\mathrm{HMW}} = \frac{1}{\hbar}\int \mathbf{A}_{\mathrm{p}} \cdot d\mathbf{r}, \tag{2.8}$$

where $\mathbf{A}_{\mathrm{p}}$ is the effective vector potential given by

$$\mathbf{A}_{\mathrm{p}} = g_{\mathrm{HMW}}\, \mathbf{B} \times \mathbf{e}_z, \tag{2.9}$$

where $g_{\mathrm{HMW}} = p$ for vaccum.

The He-McKellar-Wilkens (HMW) phase [79, 80] can be derived in a similar manner to the AC phase. We consider an electric-dipople constituting a pair of point charges $+q$ and $-q$ located at $z = +d/2$ and $z = -d/2$, where $p = qd$. If the electric-dipole moves in the x-direction with velocity $\mathbf{v}$, the two point charges $\pm q$ generate counter-propagating electric currents along x, as illustrated in Fig. 2.1(b). This gives rise to a magnetic moment in the y-direction as

$$\boldsymbol{\mu} = -g_{\mathrm{HMW}}\mathbf{v} \times \mathbf{e}_z, \tag{2.10}$$

where $g_{\mathrm{HMW}} = p$.

If an external magnetic field $\mathbf{B}$ is present, the particle has an magnetostatic potential energy $-\boldsymbol{\mu}\cdot\mathbf{B}$. Thus, the Lagrangian for the particle is given by

$$L = \frac{1}{2}m\mathbf{v}^2 + \boldsymbol{\mu}\cdot\mathbf{B}, \tag{2.11}$$

where m is a mass of the particle. As the second term is transformed as $\boldsymbol{\mu}\cdot\mathbf{B} = -g_{\rm HMW}(\mathbf{v}\times\mathbf{e}_{\rm z})\cdot\mathbf{B} = g_{\rm HMW}(\mathbf{B}\times\mathbf{e}_{\rm z})\cdot\mathbf{v}$, the Lagrangian is written as

$$L = \frac{1}{2}m\mathbf{v}^2 + \mathbf{v}\cdot\mathbf{A}_{\rm p}, \tag{2.12}$$

where $\mathbf{A}_{\rm p} = g_{\rm HMW}\mathbf{B}\times\mathbf{e}_{\rm z}$. Since Eq. (2.12) is formally equivalent to the Lagrangian of an electron in a magnetic field, $\mathbf{A}_{\rm p}$ plays the role of the effective vector potential for the electric-dipole. Therefore, the moving electric-dipole acquires the HMW phase [Eq. (4.1)].

Altenatively, this HMW phase can directly be derived from the Aharonov-Bohm (AB) phase as follows. When the dipole moves horizontally along the x-axis, from x to $x+\Delta x$, the positive and negative charges acquire Aharonov-Bohm (AB) phases given by $\theta_\pm = (\pm q/\hbar)\int_{C_\pm} d\mathbf{r}\cdot\mathbf{A}(\mathbf{r})$, where $C_\pm$ are the paths followed by the positive and negative charges, respectively. The total geometric phase for the dipole is given by $\theta_{\rm HMW} = \theta_+ + \theta_-$, and it becomes $(q/\hbar)[\int_{C_+} - \int_{C_-}]d\mathbf{r}\cdot\mathbf{A}(\mathbf{r}) = (p/\hbar)B_y(\mathbf{r})\Delta x$, where we used Stokes's theorem and $p = qd$. The result is consistent with Eqs. (4.1) and (4.2).

2.2 Ginzburg-Landau theory of Superconductivity

We review the standard Ginzburg-Landau theory [104] for superconductors, to provide a basis for comparison with the corresponding theory for dipople superfluids (Chapter 3 and 4). The Ginzburg-Landau free energy functional for conventional superconductors is given by

$$F_{\rm GL}[\Psi,\mathbf{A}] = \int d^3r\Big[\frac{1}{4m_e}\big|(-i\hbar\boldsymbol{\nabla}+2e\mathbf{A})\Psi(\mathbf{r})\big|^2 - \alpha|\Psi(\mathbf{r})|^2 + \frac{\beta}{2}|\Psi(\mathbf{r})|^4\Big] \tag{2.13}$$

where m_e is the electron mass, and e (>0) is the elementary charge. $\Psi(\mathbf{r})$ represents the superconducting order parameter and $\mathbf{B} = \boldsymbol{\nabla}\times\mathbf{A}$ represents the magnetic flux density, where $\mathbf{A}$ is the vector potential. The Ginzburg-Landau equation for the order parameter is given by

$$\frac{\delta F_{\rm GL}}{\delta\Psi^*} = \frac{1}{4m_e}(-i\hbar\boldsymbol{\nabla}+2e\mathbf{A})^2\Psi - \alpha\Psi + \beta|\Psi|^2\Psi = 0. \tag{2.14}$$

The superconducting current is described by the London equation, giving

$$\mathbf{j} = -\frac{e\hbar}{m_e}|\Psi|^2\left(\boldsymbol{\nabla}\theta + \frac{2e}{\hbar}\mathbf{A}\right) = -\frac{\delta F_{\mathrm{GL}}}{\delta \mathbf{A}}, \tag{2.15}$$

and this superconducting current produces the magnetization $\mathbf{M}$ by Maxwell equations, giving

$$\mathbf{j} = \boldsymbol{\nabla} \times \mathbf{M}. \tag{2.16}$$

By combining Eq. (2.15) with Eq. (2.16), we have $\boldsymbol{\nabla}\times\boldsymbol{\nabla}\times\mathbf{A} = -\lambda^{-2}\mathbf{A}$, where $\lambda = \sqrt{m_e/(2\mu_0 e^2|\Psi|^2)}$ is the London's penetration depth. Thus, we obtain $\boldsymbol{\nabla}^2\mathbf{B} = \lambda^{-2}\mathbf{B}$, which shows the exponential decay of the magnetic flux density (i.e. Meissner effect).

The total Gibbs free energy including magnetic field contribution is given by

$$G[\mathbf{H}(\mathbf{r}), T] = F_{\mathrm{GL}} + \int d\mathbf{r}\, \left(\frac{\mathbf{B}(\mathbf{r})^2}{2\mu_0} - \mathbf{B}(\mathbf{r})\cdot\mathbf{H}(\mathbf{r})\right). \tag{2.17}$$

The derivation is given as follows. We consider a quasi-static, isothermal process where the external magnetic field $\mathbf{H}$ is slowly introduced to the superconductors with temperature fixed. The change in the Gibbs free energy from the initial state (i) with $\mathbf{H} = 0$ to the final state (f) with $\mathbf{H}$ is given by

$$\begin{aligned} G[\mathbf{H}(\mathbf{r}), T] - G[0, T] &= -\int_{\mathrm{i}}^{\mathrm{f}} \int d\mathbf{r}\ \mathbf{B}(\mathbf{r})\cdot\delta\mathbf{H}(\mathbf{r}) \\ &= \int_{\mathrm{i}}^{\mathrm{f}} \int d\mathbf{r} \left(\frac{\mathbf{B}\cdot\delta\mathbf{B}}{\mu_0} - \mathbf{H}\cdot\delta\mathbf{B} - \mathbf{B}\cdot\delta\mathbf{H} - \mathbf{M}\cdot\delta\mathbf{B}\right) \\ &= \int d\mathbf{r}\, \left(\frac{\mathbf{B}^2}{2\mu_0} - \mathbf{B}\cdot\mathbf{H}\right) - \int_{\mathrm{i}}^{\mathrm{f}} \int d\mathbf{r}\ \mathbf{M}\cdot\delta\mathbf{B} \end{aligned} \tag{2.18}$$

We can show that the last term coincides with the change in F_{GL} by the following argument. In a quasi-static process, the infinitesimal change in the GL free energy functional is given by

$$\begin{aligned} \delta F_{\mathrm{GL}}[\Psi, \mathbf{A}] &= \int d\mathbf{r} \frac{\delta F_{\mathrm{GL}}}{\delta \mathbf{A}} \cdot \delta\mathbf{A} \\ &= -\int d\mathbf{r}\ \mathbf{j}\cdot\delta\mathbf{A} \\ &= -\int d\mathbf{r}\ (\boldsymbol{\nabla}\times\mathbf{M})\cdot\delta\mathbf{A} \\ &= -\int d\mathbf{r}\ \mathbf{M}\cdot(\boldsymbol{\nabla}\times\delta\mathbf{A}) \\ &= -\int \mathbf{M}\cdot\delta\mathbf{B}. \end{aligned} \tag{2.19}$$

We note that $\delta F_{\rm GL}/\delta\Psi = \delta F_{\rm GL}/\delta\Psi^* = 0$ throughout the process. Equations (2.18) and (2.19) lead to the Eq. (2.17).

We can readily check that self-consistent equations are derived by the variation of the total Gibbs free energy with $\mathbf{H}$ fixed: Eq. (2.14) is obtained from $\delta G/\delta\Psi = 0$ since $\delta G/\delta\Psi = \delta F_{\rm GL}/\delta\Psi$. Eq. (2.16) is derived by $\delta G/\delta\mathbf{A} = 0$, noting

$$\begin{aligned}\frac{\delta G}{\delta \mathbf{A}} &= \frac{\delta F_{\rm GL}}{\delta \mathbf{A}} + \frac{\delta}{\delta \mathbf{A}}\left(\frac{\mathbf{B}^2}{2\mu_0} - \mathbf{B}\cdot\mathbf{H}\right) \\ &= -\mathbf{j} + \frac{1}{\mu_0}\boldsymbol{\nabla}\times\boldsymbol{\nabla}\times\left(\mathbf{A} - \mathbf{A}^{\rm ext}\right) \\ &= 0, \end{aligned} \tag{2.20}$$

where we used relations $\mathbf{B} = \mu_0(\mathbf{H} + \mathbf{M})$ and $\mathbf{B} = \boldsymbol{\nabla}\times\mathbf{A}$. Here, $\mathbf{A}^{\rm ext}$ is the vector potential of the external magnetic field defined by $\mu_0\mathbf{H} = \boldsymbol{\nabla}\times\mathbf{A}^{\rm ext}$.

Chapter 3

Electric-field response in magnetic-dipole superfluids

We first focus on the magnetic-dipole superfluids under external electric field. We assume that bosons with a constant magnetic moment $\boldsymbol{\mu} = \mu \mathbf{e}_z$ form a Bose-Einstein condensate, where $\mathbf{e}_z$ is a unit vector along the direction of the magnetic dipole moment. The considered situation applies to a spin-triplet excitonic insulator and a magnon Bose-Einstein condensate, with $\mu = g\mu_B$, where $g \simeq 2$ is the Lande g-factor and μ_B is the Bohr magneton. From the standard magnon gas picture, the magnetic dipole moment of the magnon is fixed along the z-direction.

3.1 Pseudo-magnetic field by Aharonov-Casher effect

When a magnetic dipole moment $\boldsymbol{\mu} = \mu \mathbf{e}_z$ moves in an electric field $\mathbf{E}$, it acquires the Aharonov-Casher (AC) phase [28],

$$\theta_{\mathrm{AC}} = -\frac{1}{\hbar} \int \mathbf{A}_{\mathrm{m}} \cdot d\mathbf{r}, \tag{3.1}$$

where an effective vector potential is defined by

$$\mathbf{A}_{\mathrm{m}} = g_{\mathrm{AC}} \mathbf{E} \times \mathbf{e}_z. \tag{3.2}$$

The constant $g_{\mathrm{AC}}(> 0)$ represents the strength of the spin-orbit coupling, and depends on the detail of the material. In vacuum, the g_{AC} is μ/c^2, where c is the speed of light. For magnons in a typical magnetic insulator, g_{AC} greatly enhances and is typically 10^6 times as large as in vacuum [47, 48].

Being perpendicular to $\mathbf{e}_z$ [Eq. (3.2)], $\mathbf{A}_{\mathrm{m}}$ becomes a two dimensional vector with A^x_{m} and A^y_{m}

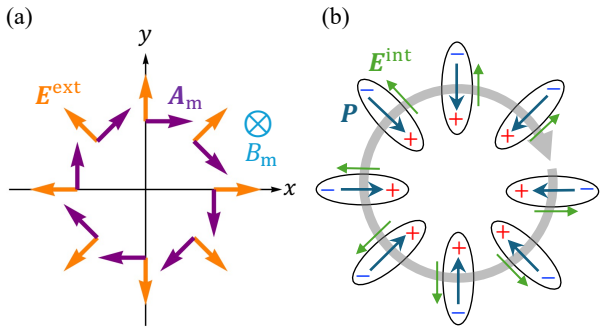


Figure 3.1: **Positive feedback effect in magnetic dipole superfluids.** Schematic figures of (a) externally applied electric field and (b) the electromagnetic response of magnetic dipoles. An external electric field $\mathbf{E}^{\mathrm{int}}$ induce effective vector potential $\mathbf{A}_{\mathrm{m}}$ of the AC phase, resulting negative pseudo-magnetic field $B_{\mathrm{m}} < 0$. The magnetic dipole experiences Lorentz force from the pseudo-magnetic field and perform cyclotron motion (circular arrow in (b)). The moving magnetic dipole then induces electric polarization $\mathbf{P}$, and generate additional electric field $\mathbf{E}^{\mathrm{int}}$, showing positive feedback effect $\mathbf{E}^{\mathrm{ext}} \cdot \mathbf{E}^{\mathrm{int}} > 0$.

components. The corresponding pseudo-magnetic field along z-direction is then written as

$$B_{\mathrm{m}} = (\boldsymbol{\nabla} \times \mathbf{A}_{\mathrm{m}})_z = -g_{\mathrm{AC}} \left(\frac{\partial E^x}{\partial x} + \frac{\partial E^y}{\partial y} \right). \tag{3.3}$$

Unlike the usual vector potential in AB phase, the effective vector potential $\mathbf{A}_{\mathrm{m}}$ does not have a gauge degrees of freedom, since it is directly expressed by the electric field.

For instance, an electric field distribution

$$\mathbf{E} = \frac{\mathcal{E}}{2}(x, y, -2z) \tag{3.4}$$

gives $\mathbf{A}_{\mathrm{m}} = (-g_{\mathrm{AC}}\mathcal{E}/2) r\, \mathbf{e}_\phi$ in the cylindrical coordinate (r, ϕ, z), resulting in a uniform pseudo-magnetic field $B_{\mathrm{m}} = -g_{\mathrm{AC}}\mathcal{E}$. Such an electric field distribution can be realized by an appropriate arrangement of external electric charges. For instance, if we put a pair of point charges $+Q$ at $\boldsymbol{r}_\pm = (0, 0, \pm l)$, the desired electric field with $\mathcal{E} \approx Q/(2\pi\varepsilon_0 l^3)$ is obtained near the origin.

3.2 Positive feedback mechanism

When a magnetic-dipole system is placed in a spatially varying electric field that induces a pseudo-magnetic field, the system responds with positive feedback, amplifying the applied electric field. Here we explain this effect through a qualitative argument based on the classical mechanics.

We consider a situation where a magnetic-dipole polarized to z axis is placed in an external electric field $\boldsymbol{E}^{\mathrm{ext}}$ given by Eq. (3.4). $\boldsymbol{E}^{\mathrm{ext}}$ is radially distributed in the xy-plane as shown in Fig. 3.1.

It induces an effective vector potential in the azimuthal direction, resulting in a negative uniform pseudo-magnetic field $B_{\rm m} < 0$ in z direction. According to the discussion in the Appendix 2.1.2, the Hamiltonian of a magnetic dipole is expressed by $H = (\mathbf{p}+\mathbf{A}_{\rm m})^2/(2m^*)$, where m^* and $\mathbf{p}$ represent the mass and the momentum of a magnetic dipole. Consequently, the dipole experiences a Lorentz force $\mathbf{F} = -\mathbf{v} \times \mathbf{B}_{\rm m}$ due to the pseudo-magnetic field and undergoes cyclotron motion [29–31], as depicted by the gray arrow in Fig. 3.1.

Generally, the motion of the magnetic dipole induces an electric dipole $\boldsymbol{p} = g_{\rm AC}\mathbf{v}\times\mathbf{e}_{\rm z}$ perpendicular to its velocity, as a reciprocal phenomenon to the AC effect [47–52]. When multiple magnetic dipoles exhibit the same circular motion, the macroscopic electric polarization $\boldsymbol{P}$ (the density of $\boldsymbol{p}$) arises in the same direction, and it generates an additional electric field $\mathbf{E}^{\rm int} = -\boldsymbol{P}/\varepsilon_0$. As shown in Fig. 3.1, $\boldsymbol{P}$ and $\boldsymbol{E}^{\rm ext}$ are oppositely oriented unlike in usual dielectric materials, indicating a negative electric susceptibility. As a result, the induced electric field $\mathbf{E}^{\rm int}$ aligns with $\mathbf{E}^{\rm ext}$, i.e., the system exhibits a positive feedback effect ($\mathbf{E}^{\rm ext}\cdot\mathbf{E}^{\rm int} > 0$). In the following sections, we demonstrate that the positive feedback effect plays a crucial role in the magnetic-dipole superfluid.

3.3 Ginzburg-Landau theory

We develop a phenomenological theory for the magnetic-dipole superfluid including the AC phase. For the sake of comparison, we also presented the phenomenological Ginzburg-Landau theory for conventional superconductors in the Sec. 2.2 to be directly compared with the following formulation for magnetic-dipole superfluids.

3.3.1 Formulation

We consider charge neutral Bose particles with a magnetic moment $\boldsymbol{\mu} = \mu\mathbf{e}_z$ forming a Bose-Einstein condensate. Utilizing an analogy to the Ginzburg-Landau theory of superconductivity or rotating atomic BEC, the free energy $F_{\rm GL}$ of the magnetic-dipole superfluid is given by

$$F_{\rm GL}[\Psi, \mathbf{A}_{\rm m}] = \int d^3\mathbf{r}\Big[\frac{1}{2m^*}\big|(-i\hbar\boldsymbol{\nabla} + \mathbf{A}_{\rm m}(\mathbf{r}))\Psi(\mathbf{r})\big|^2 - \alpha|\Psi(\mathbf{r})|^2 + \frac{\beta}{2}|\Psi(\mathbf{r})|^4\Big], \tag{3.5}$$

where m^* is the effective mass, and $\Psi(\mathbf{r}) = |\Psi(\mathbf{r})|\exp(i\theta(\mathbf{r}))$ is the order parameter, or the macroscopic wavefunction of the magnetic-dipole superfluid. We assume $\alpha > 0$ and $\beta > 0$ for the stability of the BEC. The parameter α depends on a temperature T and is given by $\alpha(T) \propto (T_c - T)^\nu$, where T_c is a critical temperature and ν is a critical exponent. The superfluid satisfies the Ginzburg-

Landau (GL) equation

$$\frac{\delta F_{\rm GL}}{\delta \Psi^*} = \frac{1}{2m^*}(-i\hbar\boldsymbol{\nabla} + \mathbf{A}_{\rm m})^2\Psi - \alpha\Psi + \beta|\Psi|^2\Psi = 0. \tag{3.6}$$

The first term in the integral of Eq. (3.5) is the kinetic energy density, and it should correspond to $n^*(m^*v^{*2}/2)$ where $n^* = |\Psi|^2$ is the the superfluid density and v^* is the velocity. Then, the associated supercurrent density, $\mathbf{j}_{\rm m} = n^*v^*$, is written as

$$\mathbf{j}_{\rm m} = \frac{\hbar}{m^*}|\Psi|^2\left(\boldsymbol{\nabla}\theta + \frac{1}{\hbar}\mathbf{A}_{\rm m}\right) = \frac{\delta F_{\rm GL}}{\delta \mathbf{A}_{\rm m}}. \tag{3.7}$$

Eq. (3.7) has an equivalent form to a conventional superconductor under mangnetic field, except that the vector potential is replaced with the effective vector potential $\mathbf{A}_{\rm m}$ for the AC effect. The supercurrent flows in the direction of the effective vector potential $\mathbf{A}_{\rm m}$, which is perpendicular to both the electric field $\mathbf{E}$ and the magnetic dipole moment $\parallel \mathbf{e}_z$.

As argued in the previous section, a current of magnetic-dipole moment induces an electric polarization [47–53]. In the present case, the polarization $\mathbf{P}$ (density of electric dipole moment) induced by the magnetic-dipole supercurrent $\mathbf{j}_{\rm m}$ is given by

$$\mathbf{P} = g_{\rm AC}\,\mathbf{j}_{\rm m} \times \mathbf{e}_z. \tag{3.8}$$

By definition, $\mathbf{P}$ does not have a z-component. The electric field can then be expressed as

$$\mathbf{E} = \mathbf{E}^{\rm ext} - \frac{\mathbf{P}}{\varepsilon_0}, \tag{3.9}$$

where $\mathbf{E}^{\rm ext}$ represents the external electric field contributed from electric charges outside the system, and ε_0 is the permittivity of free space. For simplicity, we assume the polarization of the superfluid is entirely generated by the supercurrent, ignoring the polarization of normal state. In standard terms of electromagnetism, $\mathbf{E}^{\rm ext}$ corresonds to the the electric displacement field $\mathbf{D} = \varepsilon_0\mathbf{E}^{\rm ext}$, and Eq. (3.9) is written as $\mathbf{E} = (\mathbf{D} - \mathbf{P})/\varepsilon_0$.

From Eqs. (3.2),(3.8), and (3.9), the effective vector potential is written as

$$\mathbf{A}_{\rm m} = \mathbf{A}_{\rm m}^{\rm ext} + \frac{g_{\rm AC}^2}{\varepsilon_0}\mathbf{j}_{\rm m}^{\parallel}, \tag{3.10}$$

where $\mathbf{A}_{\rm m}^{\rm ext} = g_{\rm AC}\mathbf{E}_{\rm ext} \times \mathbf{e}_z$ and $\mathbf{j}_{\rm m}^{\parallel}$ is the xy-component of $\mathbf{j}_{\rm m}$. The corresponding pseudo-magnetic

field $B_{\rm m} = (\boldsymbol{\nabla} \times \mathbf{A}_{\rm m})_z$ is given by

$$\begin{aligned} B_{\rm m} &= B_{\rm m}^{\rm ext} + \frac{g_{\rm AC}^2}{\varepsilon_0}(\boldsymbol{\nabla} \times \mathbf{j}_{\rm m}^{\parallel})_z \\ &= B_{\rm m}^{\rm ext} + \frac{g_{\rm AC}}{\varepsilon_0}\rho, \end{aligned} \tag{3.11}$$

where $\rho = -\boldsymbol{\nabla} \cdot \mathbf{P}$ is the polarization charge density. When we consider the response of the system to an external electric field $\mathbf{E}^{\rm ext}$, we solve the GL equation [Eq. (3.6)] self-consistently with Eq (3.7) and (3.10).

3.3.2 Helmholtz free energy

The same set of equations can also be derived by variation of the total Helmholtz free energy including the electrostatic field. For the magnetic-dipole superfluid, it is given by

$$F[\mathbf{D}(\mathbf{r}), T] = F_{\rm GL} + \int d\mathbf{r}\ \frac{\mathbf{D}(\mathbf{r})^2 - \mathbf{P}(\mathbf{r})^2}{2\varepsilon_0}, \tag{3.12}$$

as a functional of the external field $\mathbf{D}(\mathbf{r}) = \varepsilon_0 \mathbf{E}^{\rm ext}(\mathbf{r})$. Equation (3.12) is one of the principal results of our paper. It can be derived by considering a quasi-static process where the external electric field is slowly introduced to the dipole superfluid. The detailed calculation is provided in the Appendix B.1. It is straightforward to check that Eqs. (3.6) and (3.10) are obtained by the equilibrium conditions $\delta F/\delta\Psi = 0$ and $\delta F/\delta \mathbf{A}_{\rm m} = 0$, respectively.

3.3.3 Dimensionless equations

To highlight the essential scales of the system and relevant parameters, we rewrite the equations in a dimensionless form. Similar to the standard Ginzburg-Landau framework for superconductors, we normalize the position $\mathbf{r}$ as $\tilde{\mathbf{r}} = \mathbf{r}/\xi$ and the spatial derivative as $\tilde{\boldsymbol{\nabla}} = \xi \boldsymbol{\nabla}$, where

$$\xi = \sqrt{\frac{\hbar^2}{2m^*\alpha}} \tag{3.13}$$

is the coherence length of the superfluid. The order parameter is normalized as $\tilde{\Psi} = \Psi/\Psi_\infty$ in units of a uniform BEC value $\Psi_\infty = \sqrt{\alpha/\beta}$, the effective vector potential as $\tilde{\mathbf{A}}_{\rm m} = \mathbf{A}_{\rm m}/(\hbar/\xi)$, and energy functional as $\tilde{F}_{\rm GL} = F_{\rm GL}/(\alpha^2\xi^3/\beta)$. As a result, the superfluid free energy [Eq. (3.5)] is expressed in a dimensionless form as

$$\tilde{F}_{\rm GL} = \int d^3\tilde{r}\, |(\tilde{\boldsymbol{\nabla}} + i\tilde{\mathbf{A}}_{\rm m})\tilde{\Psi}|^2 - |\tilde{\Psi}|^2 + \frac{1}{2}|\tilde{\Psi}|^4. \tag{3.14}$$

Eq. (3.6) becomes

$$-(\tilde{\boldsymbol{\nabla}} + i\tilde{\mathbf{A}}_{\rm m})^2\tilde{\Psi} - \tilde{\Psi} + |\tilde{\Psi}|^2\tilde{\Psi} = 0. \tag{3.15}$$

The supercurrent [Eq. (3.7)], polarization [Eq. (3.8)], and polarization charge density are normalized as

$$\tilde{\mathbf{j}}_{\rm m} = |\tilde{\Psi}|^2(\tilde{\boldsymbol{\nabla}}\theta + \tilde{\mathbf{A}}_{\rm m}), \tag{3.16}$$

$$\tilde{\mathbf{P}} = \tilde{\mathbf{j}}_{\rm m} \times \mathbf{e}_z, \tag{3.17}$$

$$\tilde{\rho} = -\tilde{\boldsymbol{\nabla}} \cdot \tilde{\mathbf{P}}, \tag{3.18}$$

where $\tilde{\mathbf{j}}_{\rm m} = \mathbf{j}_{\rm m}/j_0$, $\tilde{\mathbf{P}} = \mathbf{P}/(g_{\rm AC}j_0)$ and $\tilde{\rho} = \rho/(g_{\rm AC}j_0/\xi)$ with $j_0 = \hbar\Psi_\infty^2/(m^*\xi)$. The effective vector potential, Eq. (3.10), becomes

$$\tilde{\mathbf{A}}_{\rm m} = \tilde{\mathbf{A}}_{\rm m}^{\rm ext} + \eta\tilde{\mathbf{j}}_{\rm m} \tag{3.19}$$

with

$$\eta = \frac{g_{\rm AC}^2\Psi_\infty^2}{m^*\varepsilon_0}. \tag{3.20}$$

The parameter η is a dimensionless quantity that characterizes the strength of the electrostatic coupling in the superfluid. The η depends on temperature as $\eta(T) \propto \alpha(T) \propto (T_c - T)^\nu$ according to Eq. (3.20). The pseudo-magnetic field [Eq. (3.11)] is written as

$$\begin{aligned}\tilde{B}_{\rm m} &= \tilde{B}_{\rm m}^{\rm ext} + \eta(\tilde{\boldsymbol{\nabla}} \times \tilde{\mathbf{j}}_{\rm m})_z \\ &= \tilde{B}_{\rm m}^{\rm ext} - \eta\tilde{\rho},\end{aligned} \tag{3.21}$$

where $\tilde{B}_{\rm m} = B_{\rm m}/(\hbar/\xi^2)$. In this unit, the pseudo-magnetic flux penetrating a given area becomes equal to the AC phase integrated along the boundary, and hence the dimensionless flux quanta is given by $\tilde{\phi}_{\rm m}^0 = 2\pi$.

The total free energy of Eq.(3.12) is normalized as

$$\tilde{F} = \tilde{F}_{\rm GL}[\tilde{\Psi}, \tilde{\mathbf{A}}_{\rm m}] + \eta\int d^3\tilde{r}\ \left(\tilde{\mathbf{D}}^2 - \tilde{\mathbf{P}}^2\right), \tag{3.22}$$

where $\tilde{F} = F/(\xi^3\alpha^2/\beta)$, $\tilde{\mathbf{D}} = \mathbf{D}/(g_{\rm AC}j_0)$ and $\tilde{\mathbf{E}} = \mathbf{E}/(g_{\rm AC}j_0/\varepsilon_0)$.

Equations (3.15), (3.16) and (3.19) are a set of the self-consistent equations. The latter two

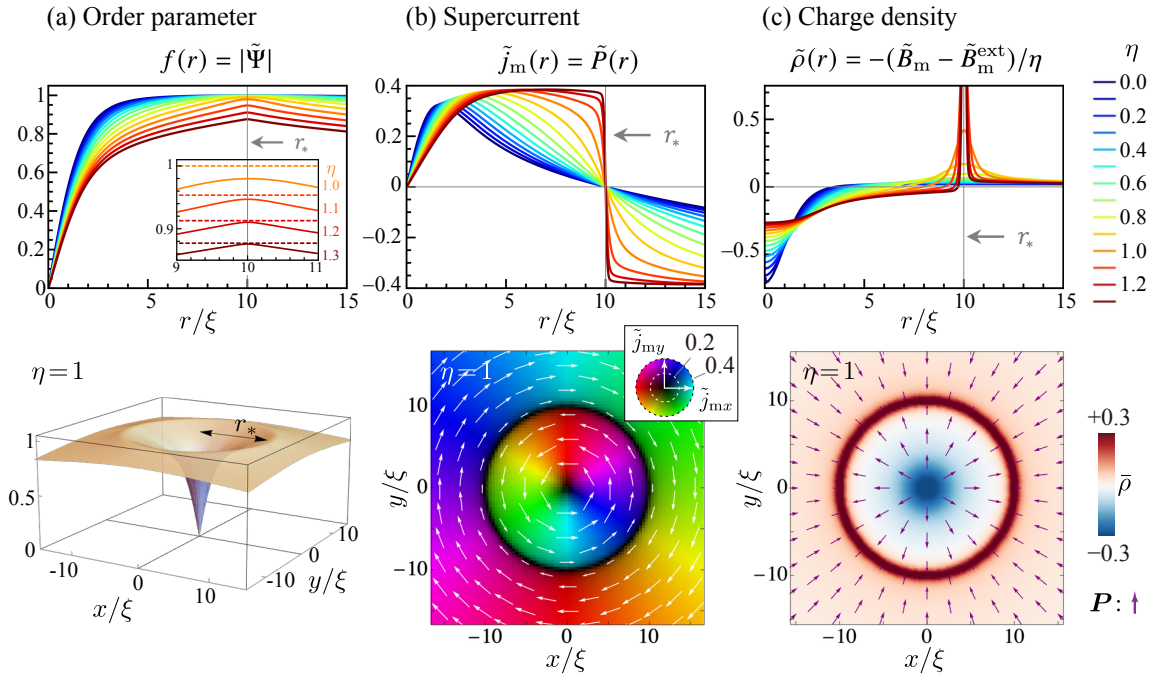


Figure 3.2: **Single vortex states in magnetic-dipole superfluids.** Self-consistent solution of a magnetic-dipole superfluid with a single vortex of $n = 1$ under $\tilde{B}_{\rm m}^{\rm ext} = -0.02(r_* = 10)$. In top panels, we plot (a) absolute order parameter $f(r) = |\tilde{\Psi}(r)|$, (b) azimuthal component of the supercurrent $\tilde{j}_{\rm m}(r)$ (equal to the radial electric polarization, $\tilde{P}(r)$), and (c) polarization charge density $\tilde{\rho}(r)$ (equal to the internal pseudo-magnetic field), where different colors correspond to different η's. Inset of (a) is a magnified plot near $r_* = 10$, where dashed lines indicate the value of $\eta^{-1/2}$. The lower panels display the two-dimensional plots of (a) $f(r)$, (b) $\tilde{\mathbf{j}}_{\rm m}(r)$ and (c) $\tilde{\rho}(r)$ on the xy plane, at the parameter of $\eta = 1$. In (b), the arrows represent the magnetic-dipole supercurrent $\tilde{\mathbf{j}}_{\rm m}(r)$, while the color and brightness indicate its direction and magnitude, respectively, as shown in the inset. In (c), the arrows represent the polarization $\tilde{\mathbf{P}}(r)$.

equations can be readily solved for $\tilde{\mathbf{j}}_{\rm m}$ and $\tilde{\mathbf{A}}_{\rm m}$ as

$$\tilde{\mathbf{j}}_{\rm m} = \frac{|\tilde{\Psi}|^2}{1 - \eta|\tilde{\Psi}|^2}(\tilde{\boldsymbol{\nabla}}\theta + \tilde{\mathbf{A}}_{\rm m}^{\rm ext}), \tag{3.23}$$

$$\tilde{\mathbf{A}}_{\rm m} = \frac{1}{1 - \eta|\tilde{\Psi}|^2}(\eta|\tilde{\Psi}|^2\tilde{\boldsymbol{\nabla}}\theta + \tilde{\mathbf{A}}_{\rm m}^{\rm ext}). \tag{3.24}$$

An important observation is that the presence of $\eta\,(> 0)$ enhances the supercurrent and the vector potential by decreasing the denominator $1-\eta|\tilde{\Psi}|^2$. This is the positive feedback effect argued in the "Magnetic-dipole superfluids" subsection in Results. The equations also imply a singular behavior when the denominator vanishes, i.e., $\eta|\tilde{\Psi}|^2 = 1$. This will be discussed in the next subsection.

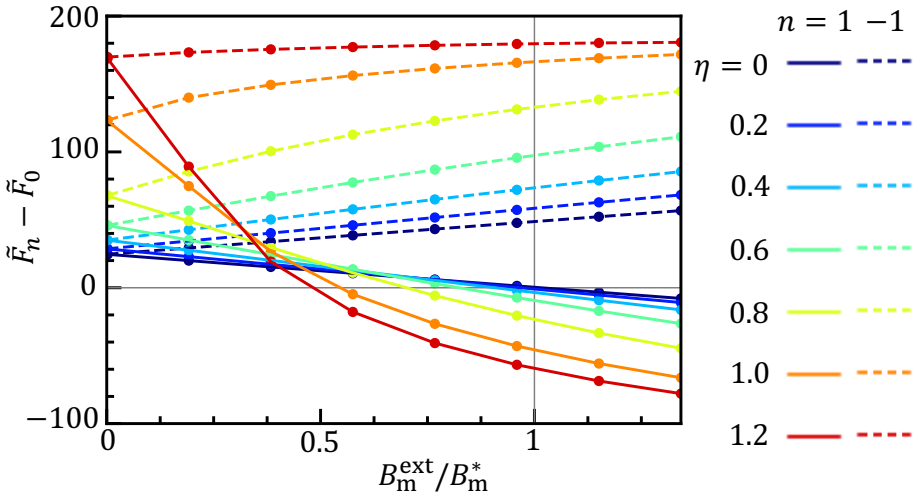


Figure 3.3: **Free energy of vortex states in the magnetic dipole superfluid.** Relative Helmholtz free energy of single vortex states $n = 1$ (solid curves) and single anti-vortex states $n = -1$ (dashed curves) compared to the uniform $n = 0$ state, as a function of the external pseudo-magnetic field $B_{\rm m}^{\rm ext}$. Colors represent the value of η.

3.4 Single-vortex state

In the following, we consider an infinitely-large magnetic-dipole superfluid under an external field of $\tilde{\mathbf{A}}_{\rm m}^{\rm ext} = (-|\tilde{B}_{\rm m}^{\rm ext}|r/2)\mathbf{e}_\phi$, which gives a uniform pseudo-magnetic field $B_{\rm m}^{\rm ext}$. (See the "Magnetic-dipole superfluids" subsection in Results.) Here we set $\tilde{B}_{\rm m}^{\rm ext} = -0.02$ (along $-z$ direction). We assume a superfluid solution of the form

$$\tilde{\Psi}(r, \phi, z) = f(r)e^{in\phi} \tag{3.25}$$

with a single vortex of $n = +1$ along the z-axis. We solve the set of self-consistent equations [Eqs. (3.6), (3.7) and (3.10)] by a numerical iteration. (See the "Technical details of self-consistent numerical calculations" subsection in Methods.) The results for different η parameters are summarized in Fig. 3.2. Here we plot (a) the absolute order parameter $f(r) = |\tilde{\Psi}(r)|$, (b) the azimuthal component of the supercurrent $\tilde{j}_{\rm m}(r)$, which is equal to the radial component of electric polarization, $\tilde{P}(r)$, and (c) polarization charge density $\tilde{\rho}(r)$, which is related to the internal pseudo-magnetic field $\tilde{B}_{\rm m}^{\rm int} = \tilde{B}_{\rm m} - \tilde{B}_{\rm m}^{\rm ext}$ by $\tilde{\rho} = -\tilde{B}_{\rm m}^{\rm int}/\eta$. The lower panels display the two-dimensional plots of the distribution of $|\tilde{\Psi}|$, $\tilde{\mathbf{j}}_{\rm m}$, $\tilde{\rho}$ on the xy plane at $\eta = 1$. In the plot of $\tilde{\mathbf{j}}_{\rm m}$, the color and brightness indicate its direction and magnitude, respectively.

First, we focus on $\eta = 0$ (blue curve in Fig. 3.2), where the electrostatic feedback is absent. In this case, the supercurrent [Eq. (3.23)] is given by $\tilde{\mathbf{j}}_{\rm m} = |\tilde{\Psi}|^2(\tilde{\boldsymbol{\nabla}}\theta + \tilde{\mathbf{A}}_{\rm m}^{\rm ext})$ where $\tilde{\boldsymbol{\nabla}}\theta = (1/r)\mathbf{e}_\phi$. Its azimuthal component then becomes $\tilde{j}_{\rm m}(r) = f(r)^2(1/r - |\tilde{B}_{\rm m}^{\rm ext}|r/2)$, which vanishes at the radius

$r_* \equiv \sqrt{2/|\tilde{B}_{\rm m}^{\rm ext}|}$ (= 10 in the present case). The r_* is the radius such that the pseudo-magnetic flux penetrating the region $r < r_*$ is equal to a quantum flux $\tilde{\phi}_{\rm m}^0 = 2\pi$.

As the parameter η is increased from zero, we observe that the vanishing point of $\tilde{\mathbf{j}}_{\rm m}$ still remains at $r = r_*$, while its slope at $r = r_*$ becomes gradually steeper, as seen in Fig. 3.2(b). This is expected from Eq. (3.23) where the supercurrent amplitude is enhanced by the denominator $1 - \eta|\tilde{\Psi}|^2$. In $\eta \gtrsim 1$, interestingly, $\tilde{\mathbf{j}}_{\rm m}(r)$ becomes a step-like function, i.e., the direction of the azimuthal supercurrent abruptly changes at $r = r_*$. Consequently, the pseudo-magnetic field exhibits a sharp peak according to the relation $B_{\rm m} - B_{\rm m}^{\rm ext} \propto \boldsymbol{\nabla} \times \mathbf{j}_{\rm m}$ [Eq. (3.21)], which is clearly observed in Fig. 3.2(c). In terms of electric quantities, this corresponds to a high magnitude of $\boldsymbol{\nabla} \cdot \mathbf{P}$, i.e., a sharply-localized polarization charge density at $r = r_*$. As η increases beyond 1, the width of the discontinuous wall at $r = r^*$ becomes extremely narrow, and the charge density as well as the pseudo magnetic field diverge.

The step-like behavior of $\tilde{j}_{\rm m}(r)$ in $\eta \gtrsim 1$ can be explained by vanishing denominator $1 - \eta|\tilde{\Psi}|^2$ in Eq. (3.23). In the present case, Eq. (3.23) is written as

$$\tilde{j}_{\rm m}(r) = \frac{1}{\frac{1}{f(r)^2} - \eta}\left(\frac{1}{r} - \frac{\left|B_{\rm m}^{\rm ext}\right|}{2} r\right). \tag{3.26}$$

In the numerical solutions presented in Fig. 3.2, the $f(r)$ of $\eta \gtrsim 1$ exhibits a kink structure in the vicinity of r_*, which is well described by

$$f(r) = \eta^{-1/2} - a|r - r_*| \quad (a > 0). \tag{3.27}$$

Then the denominator of Eq. (3.26) is written as $\frac{1}{f(r)^2} - \eta \approx 2\eta^{3/2} a|r - r_*|$ in the lowest order in $r - r_*$. Noting the bracket in Eq. (3.26) can be approximated by $(-2/r_*^2)(r - r_*)$, we end up with a step function

$$\tilde{j}_{\rm m}(r) = \frac{1}{\eta^{3/2} a r_*^2} \mathrm{sgn}(r_* - r), \tag{3.28}$$

where $\mathrm{sgn}(x) \equiv x/|x|$. Here we note that the maximum of $f(r)$ is $\eta^{-1/2}$ [Eq. (3.27)], i.e., the $f(r)$ is tuned in such a way that the denominator of Eq. (3.26) vanishes right at $r = r_*$. This cancels with the original zero of the supercurrent, resulting in a step function. In the actual numerical result, the kink of $f(r)$ at $r = r_*$ is rounded so that the maximum is slightly lower than $\eta^{-1/2}$ as observed in the inset of Fig. 3.2(a), which prevents the denominator from completely vanishing. Consequently, the step structure in $\tilde{j}_{\rm m}$ is smoothed into a continuous, yet rapidly-changing function.

It should also be noted that the total flux inside the radius $r = r^*$ remains quantized even

when the internal field $B_{\rm m}^{\rm int} = B_{\rm m} - B_{\rm m}^{\rm ext}$ is included. This can be understood by the following consideration: By applying the Stokes theorem to Eq. (3.21), the flux of the internal field in $r < r_*$ becomes $\int_{r<r_*} B_{\rm m}^{\rm int} d^2r \propto \oint_{r=r_*} \mathbf{j}_{\rm m} \cdot d\mathbf{r}$, which vanishes since $\mathbf{j}_{\rm m} = 0$ at $r = r_*$. Therefore, the total flux inside r_* is contributed solely by the external field $B_{\rm m}^{\rm ext}$, which is quantized by definition. Zero flux of $B_{\rm m}^{\rm int}$ inside the radius r_* is equivalent to a zero net charge within the region.

It should also be emphasized that the domain wall found in our calculation differs from the conventional case in the following way: In superconducting domain walls, the order parameter undergoes an abrupt π phase change, causing it to vanish at the domain wall [105]. In contrast, in the singular domain wall of magnetic-dipole superfluids, the order parameter does not vanish; instead, its derivative (i.e., the supercurrent) vanishes and changes sign.

To demonstrate the energetic advantage of the vortex state in pseudo-magnetic fields, we investigate the total free energy F with and without a vortex. Here we consider a finite system of the disc with radius $R = 40$, and obtain the self-consistent solutions with no vortex ($n = 0$), a single vortex ($n = 1$), a single anti-vortex ($n = -1$) at the center of the disc. We impose a boundary condition such that the order parameter vanishes at the edge of the disc $r = R$. For the obtained solutions, we calculate the total free energy of the system F given by Eq. (3.12).

Figure 3.3 plots the relative total free energy of $n = 1$ (solid curves) and $n = -1$ (dashed curves) compared to the $n = 0$ state, as a function of the external pseudo-magnetic field $B_{\rm m}^{\rm ext}$. The different colors correspond to different η. Let us first consider the case of $\eta = 0$ (blue curve), which corresponds to a standard superfluid without the electrostatic feedback effect. At $\tilde{B}_{\rm m}^{\rm ext} = 0$, the uniform solution ($n = 0$) is the ground state, while the vortex states ($n = \pm 1$) are degenerate in higher energy. When $\tilde{B}_{\rm m}^{\rm ext}$ is increased, the relative energy of the $n = 1$ state decreases, and it finally becomes the lowest at $B = B_{\rm m}^*(R) \equiv (1 + 2\log R)/(1 + R^2)$. The critical field $B_{\rm m}^*(R)$ can be regarded as a pseudo-magnetic field at which the system of size R allows a single vortex to enter. The anti-vortex state ($n = -1$) is always higher in energy as naturally expected.

When we increase η, the critical field at which the $n = 1$ state becomes stable monotonically decreases, i.e., the $n = 1$ vortex state is stabilized in a smaller field. It is stark contrast to the typical behaviors of superconductivity, where the critical field H_{c1} increases as the coupling to the electromagnetic field increases [104]. This corresponds to a transition from type II regime with the formation of the vortices to the type I regime where the Meissner effect occurs.

3.5 Vortex lattice

When the pseudo-magnetic field is much greater than $B^*_{\rm m}(R)$, we expect that multiple vortices enter the superfluid, forming of a vortex lattice. Here we demonstrate the emergence of a vortex lattice in a dipole superfluid by numerically solving Eqs. (3.15), (3.16) and (3.19) self-consistently. We assume a triangular lattice with primitive lattice vectors $\mathbf{a}_1 = a(1,0)$ and $\mathbf{a}_2 = a(1/2, \sqrt{3}/2)$ where a is the lattice constant. The lattice constant a is determined by the requirement that the unit cell contains exactly a quantum flux $\tilde{\phi}^0_{\rm m} = 2\pi$, giving $a^2 = 2\pi r_*^2/\sqrt{3}$.

We assume a periodic current profile $\mathbf{j}_{\rm m}(\mathbf{r} + \mathbf{a}_i) = \mathbf{j}_{\rm m}(\mathbf{r})$, which ensures $\mathbf{A}^{\rm int}_{\rm m}(\mathbf{r}) = \mathbf{A}^{\rm int}_{\rm m}(\mathbf{r} + \mathbf{a}_i)$ by Eq. (3.19). Since the periodic vector potential can only give zero flux on average, the total pseudo-magnetic flux is contributed solely by the external field $B^{\rm ext}_{\rm m}$. Therefore, we can assume that the total vector potential, including the external field, obeys the periodicity,

$$\mathbf{A}_{\rm m}(\mathbf{r} + \mathbf{L}) = \mathbf{A}_{\rm m}(\mathbf{r}) + \frac{B^{\rm ext}_{\rm m}}{2}\mathbf{e}_z \times \mathbf{L} \tag{3.29}$$

where $\mathbf{L}(l_1, l_2) = l_1\mathbf{a}_1 + l_2\mathbf{a}_2$ is a lattice translation vector with integer l_i. The order parameter then satisfies the magnetic Bloch condition,

$$\Psi(\mathbf{r} + \mathbf{L}) = \Psi(\mathbf{r}) \exp\left(-i\frac{B^{\rm ext}_{\rm m}}{2}(\mathbf{e}_z \times \mathbf{L}) \cdot \mathbf{r} + i\pi(l_1 + l_2 + l_1 l_2)\right). \tag{3.30}$$

The single-valuedness of the order parameter is guaranteed when unit cell spanned by $\mathbf{a}_1$ and $\mathbf{a}_2$ accommodates an integer mutiple of flux quanta. We solve the self-consistent equation by a numerical iteration with the periodic boundary condition of Eqs.(3.29) and (3.30), starting from an initial state with a single vortex per unit cell.

Figure 3.4 summarizes the obtained superfluid vortex lattice for $\eta = 0.8$, 1 and 1.1, in $\tilde{B}^{\rm ext}_{\rm m} = -0.02$. Each figure presents spatial maps of (a) the absolute order parameter $f(\mathbf{r})$, (b) the supercurrent $\tilde{\mathbf{j}}_{\rm m}(\mathbf{r})$, and (c) the charge density $\tilde{\rho}(\mathbf{r})\,(= -\eta\tilde{B}^{\rm int}_{\rm m}(\mathbf{r}))$, respectively. We observe that the single vortex structure argued in the previous section are periodically arranged in a consistent manner. The supercurrent $\mathbf{j}_{\rm m}$ circulates in the counterclockwise direction in each cell [Fig. 3.4(b)], or equivalently, the polarization $\mathbf{P}$ is arranged radially with respect to the vortex. When η exceeds 1, significantly, the supercurrent distribution extends upto the edge of the honeycomb unit cell, and its direction abruptly changes across the domain wall as in the single vortex case. As a result, the polarization charge (i.e., the internal pseudo-magnetic field) is sharply concentrated at the domain wall, forming a bold honeycomb domain-wall network as seen in Fig. 3.4(c). We also have negative polarization charge localized around the vortex cores, which exactly cancels with those on

the domain wall, resulting in a zero net charge. Equivalently, the integral of $B^{\rm int}$ over a unit cell is vanishing, so that the total pseudo-magnetic flux remains per unit cell equal to that of the external field $B_{\rm m}^{\rm ext}$.

We have also systematically performed the same self-consistent calculations for different angles ranging from 60° (triangular lattice) to 90° (square lattice). We find that the triangular vortex lattice always has the lowest free energy for all values of η.

If we vary $\tilde{B}_{\rm m}$ within the range $|\tilde{B}_{\rm m}| \ll 1$, it primarily affects the size of the vortex lattice while preserving its qualitative features. However, when $\tilde{B}_{\rm m}$ becomes large, on the order of 1, we expect the vortex lattice to melt into a liquid phase, similar to other superfluid systems [106].

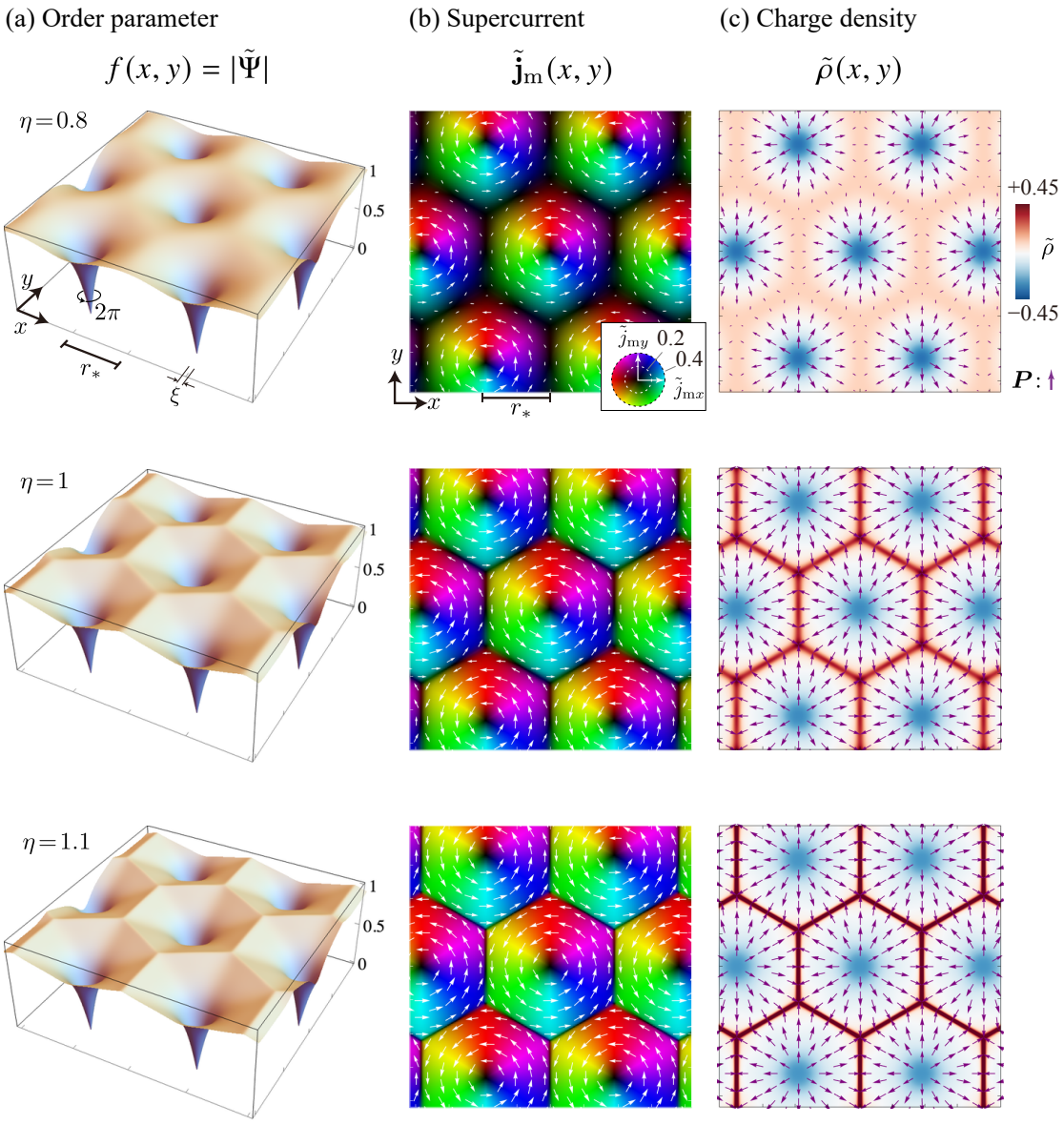


Figure 3.4: **Vortex lattices in magnetic-dipole superfluids.** Self-consistent vortex lattice of a magnetic-dipole superfluid for $\eta = 0.8$, 1 and 1.1, in $\tilde{B}_{\rm m}^{\rm ext} = -0.02$. Each figure presents spatial maps of (a) the absolute order parameter $f(\mathbf{r}) = |\tilde{\Psi}(\mathbf{r})|$, (b) the supercurrent $\tilde{\mathbf{j}}_{\rm m}(\mathbf{r})$, and (c) the charge density $\tilde{\rho}(\mathbf{r})\,(= -\tilde{B}_{\rm m}^{\rm int}(\mathbf{r})/\eta)$, respectively. In (b), the arrows represent the magnetic-dipole supercurrent $\tilde{\mathbf{j}}_{\rm m}(r)$, while the color and brightness indicate its direction and magnitude, respectively, as shown in the inset.

Chapter 4

Magnetic-field response in electric-dipole superfluids

The above argument for magnetic-dipole superfluids can be directly extended to electric dipoles, where the roles of electric and magnetic fields reversed. Such a situation can be realized in excitonic condensates, where excitons (bound states of an electron and a hole) are charge-neutral and possess an electric dipole moment [63–78, 107].

In the following, we present a phenomenological theory for electric-dipole superfluids interacting with a magnetic field, paralleling the discussion of magnetic-dipole superfluids in the previous sections. However, the electric-dipole superfluids show distinct behavior, owing to its negative feedback effect, while the magnetic-dipole superfluids show positive feedback effect.

4.1 Pseudo-magnetic field by He-McKellar-Wilkens effect

While the magnetic dipole interacts with the electric field through the AC phase, the electric dipole $\mathbf{p} = p\mathbf{e}_z$ interacts with the magnetic flux density $\mathbf{B}$ by means of the He-McKellar-Wilkens (HMW) phase [77–80, 99–103],

$$\theta_{\mathrm{HMW}} = \frac{1}{\hbar} \int \mathbf{A}_{\mathrm{p}} \cdot d\mathbf{r}, \tag{4.1}$$

where $\mathbf{A}_{\mathrm{p}}$ is the effective vector potential given by

$$\mathbf{A}_{\mathrm{p}} = g_{\mathrm{HMW}}\, \mathbf{B} \times \mathbf{e}_z, \tag{4.2}$$

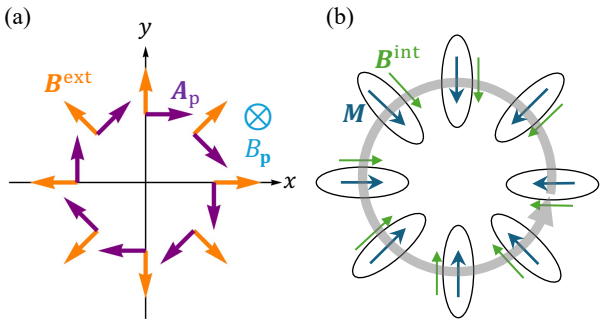


Figure 4.1: **Negative feedback effect in electric dipole superfluids.** Schematic figures of (a) externally applied magnetic field and (b) the electromagnetic response of electric dipoles, which correspond to Fig. 3.1 for magnetic dipoles. An external magnetic field $\mathbf{B}^{\mathrm{ext}}$ (orange) induce effective vector potential $\mathbf{A}_{\mathrm{p}}$ (purple) of HMW phase, resulting negative pseudo-magnetic field $B_{\mathrm{p}} < 0$. The electric dipole experiences Lorentz force from the pseudo-magnetic field and perform cyclotron motion (gray). The moving electric dipole induces a magnetization $\mathbf{M}$, and they generate additional magnetic field $\mathbf{B}^{\mathrm{int}}$, showing negative feedback effect $\mathbf{B}^{\mathrm{ext}} \cdot \mathbf{B}^{\mathrm{int}} < 0$.

where $g_{\mathrm{HMW}} = p$ for vaccum. A simple derivation of HMW phase is presented in the Appendix 2.1.3. The corresponding pseudo-magnetic field along z-direction is then written as

$$B_{\mathrm{p}} = (\boldsymbol{\nabla} \times \mathbf{A}_{\mathrm{p}})_z = -g_{\mathrm{HMW}} \left(\frac{\partial B^x}{\partial x} + \frac{\partial B^y}{\partial y} \right). \tag{4.3}$$

Here the pseudo-magnetic field is given by a spatially-dependent magnetic field. In the following, $\mathbf{B}$ and $\mathbf{B}^{\mathrm{ext}}$ represent real magnetic fields, not pseudo-magnetic fields.

4.2 Negative feedback mechanism

In contrast to the magnetic dipole case, the electric dipole exhibits the negative feedback against the external field. Figure 4.1 shows the schematic figure illustrating the response of electric dipoles, corresponding to Fig. 3.1 for magnetic dipoles. Here we apply radially-distributed magnetic field $\boldsymbol{B}^{\mathrm{ext}}$, which gives the pseudo-magnetic field $\boldsymbol{B}_p$ in the $-z$ direction. According to the Hamiltonian $H = (\mathbf{p} - \mathbf{A}_{\mathrm{p}})^2/(2m^*)$, the electric-dipole experiences a Lorentz force $\mathbf{F} = +\mathbf{v} \times \mathbf{B}_{\mathrm{p}}$ due to the pseudo-magnetic field, leading to the cyclotron motion. The motion of the electric dipoles generates a magnetic-dipole $\boldsymbol{\mu} = -g_{\mathrm{HMW}} \mathbf{v} \times \mathbf{e}_{\mathrm{z}}$, giving magnetization $\boldsymbol{M}$ (the density of $\boldsymbol{\mu}$). The $\boldsymbol{M}$ and $\boldsymbol{B}_{\mathrm{ext}}$ are oppositely oriented, indicating a diamagnetic response. This aligns with the negative dielectric response in the magnetic dipole case. The magnetization contributes to the additional magnetic field $\mathbf{B}^{\mathrm{int}} = \mu_0 \boldsymbol{M}$. Since $\mathbf{B}^{\mathrm{ext}} \cdot \mathbf{B}^{\mathrm{int}} < 0$, the feedback is negative.

This negative feedback effect contrasts with the positive feedback effect in the magnetic-dipole system. The opposite features are due to the fact that the electric field in the magnetic-dipole

case corresponds to H-field (not B-field) in the electric-dipole case, and that generally H-field and B-field induced by magnetic dipoles are oppositely directed (e.g., in magnetic materials). Indeed, if we replace + and − charges of induced electric dipole in Fig. 3.1 with N and S magnetic monopoles, we reproduce the situation of Fig. 4.1, where the induced H-field is oriented outward, similar to $\mathbf{E}^{\rm int}$ in Fig. 3.1. Therefore the induced B-field points inward.

4.3 Ginzburg-Landau theory

4.3.1 Formulation

We assume that the Ginzburg-Landau free energy functional for electric-dipole superfluids is given by

$$F_{\rm GL}[\Psi, \mathbf{A}_{\rm p}] = \int d^3r \Big[\frac{1}{2m^*} \big| (-i\hbar\boldsymbol{\nabla} - \mathbf{A}_{\rm p})\Psi(\mathbf{r}) \big|^2 - \alpha |\Psi(\mathbf{r})|^2 + \frac{\beta}{2} |\Psi(\mathbf{r})|^4 \Big], \tag{4.4}$$

where m^* is the effective mass of a quasiparticle having an electric dipole and $\Psi(\mathbf{r})$ is the order parameter. The Ginzburg-Landau equation is written as

$$\frac{\delta F_{\rm GL}}{\delta \Psi^*} = \frac{1}{2m^*}(-i\hbar\boldsymbol{\nabla} - \mathbf{A}_{\rm p})^2\Psi - \alpha\Psi + \beta|\Psi|^2\Psi = 0. \tag{4.5}$$

The supercurrent is expressed as

$$\mathbf{j}_{\rm p} = \frac{\hbar}{m^*}|\Psi|^2(\boldsymbol{\nabla}\theta - \frac{1}{\hbar}\mathbf{A}_{\rm p}) = -\frac{\delta F_{\rm GL}}{\delta \mathbf{A}_{\rm p}}. \tag{4.6}$$

Just as the current of a magnetic dipole induces electric polarization, the current of electric dipole $\mathbf{j}_{\rm p}$ induces the magnetization by

$$\mathbf{M} = g_{\rm HMW}\, \mathbf{e}_z \times \mathbf{j}_{\rm p}. \tag{4.7}$$

A brief derivation of this relation is presented in the "Geometric phases for dipoles" subsection in Methods. The magnetic flux density can be expressed as

$$\mathbf{B} = \mathbf{B}^{\rm ext} + \mu_0 \mathbf{M}. \tag{4.8}$$

where $\mathbf{B}^{\rm ext}$ is the external magnetic flux density, and μ_0 is the permeability. In the standard notation of electromagnetism, $\mathbf{B}^{\rm ext}$ corresponds to the magnetic field $\mathbf{H} = \mathbf{B}^{\rm ext}/\mu_0$, and Eq. (4.8) is written as $\mathbf{B} = \mu_0(\mathbf{H} + \mathbf{M})$. From Eqs. (4.2), (4.7), and (4.8), the total magnetic field induces

the effective vector potential

$$\mathbf{A}_{\rm p} = \mathbf{A}_{\rm p}^{\rm ext} + \mu_0 g_{\rm HMW}^2 \mathbf{j}_{\rm p}, \tag{4.9}$$

with $\mathbf{A}_{\rm p}^{\rm ext} = g_{\rm HMW}\, \mathbf{B}^{\rm ext} \times \mathbf{e}_z$.

4.3.2 Gibbs free energy

Equations (4.5) and (4.9) can alternatively be derived by variation of the total free energy including the magnetic field. In the present case, it is appropriate to use the Gibbs free energy $G[\mathbf{H}(\mathbf{r}), T] = F[\mathbf{B}(\mathbf{r}), T] - \int d\mathbf{r}\ \mathbf{B}(\mathbf{r}) \cdot \mathbf{H}(\mathbf{r})$ rather than the Helmholtz free energy $F[\mathbf{B}(\mathbf{r}), T]$, since the external magnetic field $\mathbf{H}$ is fixed. According to the argument of the Appendix B.2, the Gibbs free energy is written as

$$G[\mathbf{H}(\mathbf{r}), T] = F_{\rm GL} + \int d\mathbf{r}\ \left(\frac{\mathbf{B}(\mathbf{r})^2}{2\mu_0} - \mathbf{B}(\mathbf{r}) \cdot \mathbf{H}(\mathbf{r}) \right). \tag{4.10}$$

It is straightforward to check that Eqs. (4.5) and (4.9) are obtained by the equilibrium conditions $\delta G/\delta \Psi = 0$ and $\delta G/\delta \mathbf{A}_{\rm p} = 0$, respectively

4.3.3 Dimensionless equations

Similar to the argument for magnetic-dipole systems, the equations (4.6) and (4.9) can be expressed in a dimensionless form as,

$$\tilde{\mathbf{j}}_{\rm p} = |\tilde{\Psi}|^2 (\tilde{\nabla}\theta - \tilde{\mathbf{A}}_{\rm p}), \quad \tilde{\mathbf{A}}_{\rm p} = \tilde{\mathbf{A}}_{\rm p}^{\rm ext} + \eta_{\rm p} \tilde{\mathbf{j}}_{\rm p}, \tag{4.11}$$

where the variables with tilde represent dimensionless quantities and we defined a dimensionless parameter

$$\eta_{\rm p} = \frac{\mu_0 g_{\rm HMW}^2 \Psi_\infty^2}{m^*}, \tag{4.12}$$

which corresponds to η for magnetic-dipole supserfluids. The two equations Eqs. (4.11) can be solved for $\tilde{\mathbf{j}}_{\rm p}$ and $\tilde{\mathbf{A}}_{\rm p}$ as

$$\tilde{\mathbf{j}}_{\rm m} = \frac{|\tilde{\Psi}|^2}{1 + \eta_{\rm p} |\tilde{\Psi}|^2} (\tilde{\boldsymbol{\nabla}}\theta - \tilde{\mathbf{A}}_{\rm p}^{\rm ext}), \tag{4.13}$$

$$\tilde{\mathbf{A}}_{\rm p} = \frac{1}{1 + \eta_{\rm p} |\tilde{\Psi}|^2} (\eta_{\rm p} |\tilde{\Psi}|^2 \tilde{\boldsymbol{\nabla}}\theta + \tilde{\mathbf{A}}_{\rm p}^{\rm ext}). \tag{4.14}$$

In contrast to the corresponding formula for the magnetic-dipole case, Eqs. (3.23) and (3.24), $\eta_{\rm p}$ enters with positive sign in the denominator $1 + \eta_{\rm p} |\tilde{\Psi}|^2$. Therefore the $\eta_{\rm p} > 0$ gives s a negative feedback reducing the applied field.

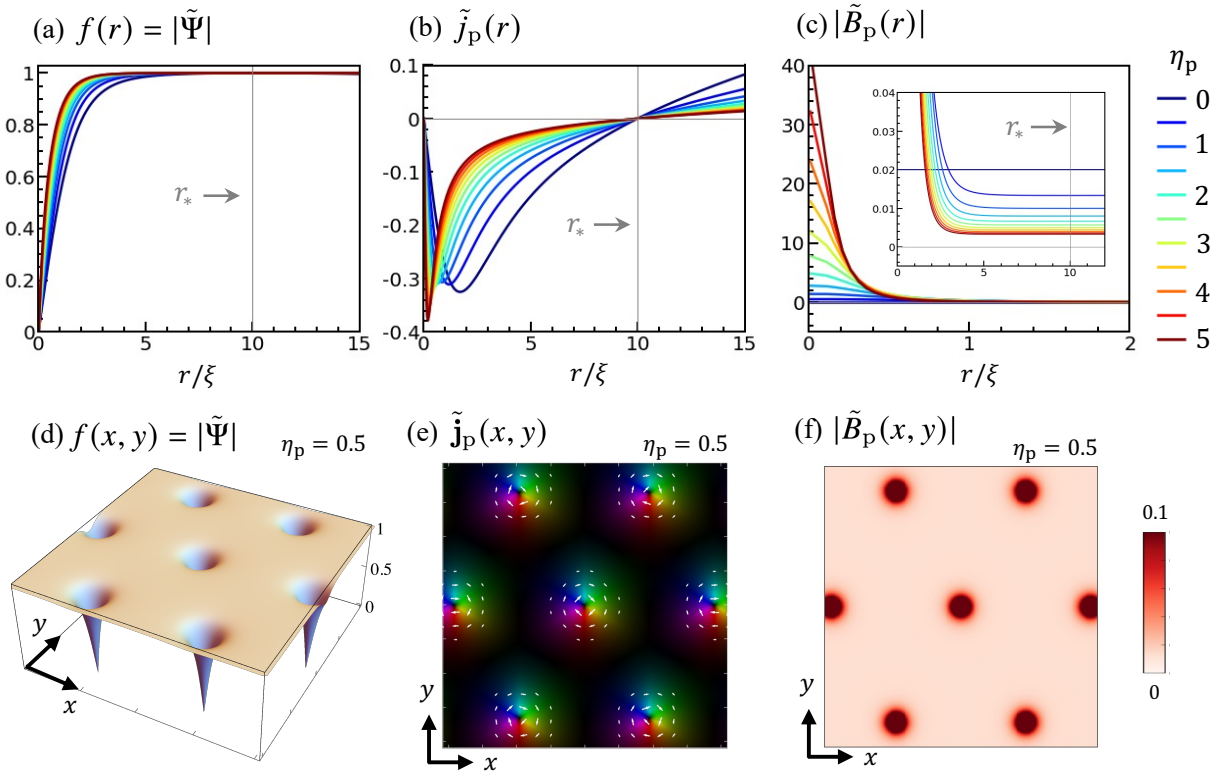


Figure 4.2: **Vortex states in electric-dipole superfluids.** In top panels, self-consistent solutions of an electric-dipole superfluid with a single vortex of $n = -1$ under $\tilde{B}_{\rm p}^{\rm ext} = -0.02$ ($r_* = 10$) are summarized. We plot (a) absolute order parameter $f(r) = |\tilde{\Psi}(r)|$, (b) azimuthal component of the supercurrent $\tilde{j}_{\rm p}(r)$ (equal to the radial magnetization, $\tilde{M}(r)$), and (c) absolute value of total pseudo-magnetic field $|\tilde{B}_{\rm p}(r)|$, where different colors correspond to different $\eta_{\rm p}$'s. Inset of (c) is a magnified plot near $|\tilde{B}_{\rm p}(r)| = 0$. In lower panels, self-consistent vortex lattice of an electric-dipole superfluid under $\tilde{B}_{\rm p}^{\rm ext} = -0.02$ ($r_* = 10$) are summarized. We display the two-dimensional plots of of (d) $f(x,y) = |\tilde{\Psi}(x,y)|$, (e) $\tilde{\mathbf{j}}_{\rm p}(x,y)$ and (f) $|\tilde{B}_{\rm p}(x,y)|$ on the xy plane, at the parameter of $\eta = 0.5$. The colors and brightness in (e) indicate the direction and magnitude of the supercurrent $\tilde{\mathbf{j}}_{\rm p}(x,y)$, respectively.

4.4 Single-vortex state

When an electric-dipole superfluid is subjected to a pseudo-magnetic field B_p (a spatially-dependent magnetic field), the system also forms a vortex lattice, while the electro-magnetic field texture is completely distinct from the case of magnetic-dipole superfluids due to the negative feedback effect.

Here, we perform analyses of a single vortex state and a vortex lattice in the electric-dipole superfluid, aligning with the corresponding calculations for the magnetic-dipole cases. First, we consider a single vortex state under an external field of $\tilde{\mathbf{A}}_{\rm p}^{\rm ext} = (-|\tilde{B}_{\rm p}^{\rm ext}|r/2)\mathbf{e}_\phi$ with $\tilde{B}_{\rm p}^{\rm ext} = -0.02$. We assume an anti-vortex state $\tilde{\Psi}(r,\phi,z) = f(r)e^{-i\phi}$, where the negative sign in the phase factor corresponds to the negative sign of the effective vector potential in Eq. (4.6). In Fig. (4.2), we plot (a) the absolute value of the order parameter $f(r) = |\tilde{\Psi}(r)|$, (b) the azimuthal component of the

supercurrent $\tilde{j}_{\rm p}(r)$, which is equal to the radial component of magnetization, $\tilde{M}(r)$, and (c) the abolute value of pseudo-magnetic field $|\tilde{B}_{\rm p}(r)|$, for different $\eta_{\rm p}$ parameters.

As seen in Fig. 4.2(b), the supercurrent is suppressed owing to the negative feedback effect (i.e. the denominator $1+\eta_{\rm p}|\tilde{\Psi}|^2$ in Eq. (4.13)). This behavior is stark contrast to magnetic-dipole superfluids, where the supercurrent is amplified by the positive feedback effect. Furthermore, as is shown in Fig. 4.2(c), the pseudo-magnetic field is sharply concentrated at the vortex core, whereas away from the core ($r \gg \xi$), it converges to a nonzero constant,

$$\tilde{B}_{\rm p}(r) \approx \frac{1}{1+\eta_{\rm p}} \tilde{B}_{\rm p}^{\rm ext} \quad (r \gg \xi). \tag{4.15}$$

This equation is obtained by taking the curl of Eq. (4.14) with $|\tilde{\Psi}(r)|^2 = 1$. It is worth noting that the total flux inside the radius $r^* \equiv \sqrt{2/|\tilde{B}_{\rm p}^{\rm ext}|}(=10)$ is always quantized, as demonstrated by the same reasoning presented in the previous section for magnetic-dipole superfluids.

4.5 Vortex lattice

We also calculate vortex lattice states of electric-dipole superfluids, in the same manner as described in the "Vortex lattices" subsection in Results. In Fig. 4.2, we show the plots of the distributions of (d) $f(x,y) = |\tilde{\Psi}(x,y)|$, (e) $\tilde{\mathbf{j}}_{\rm p}(x,y)$, (f) $|\tilde{B}_{\rm p}(x,y)|$ on the xy plane at $\eta = 0.5$. We observe that the single-vortex structures are periodically arranged in a consistent manner; the pseudo-magnetic field is primarily concentrated around the vortices and remains nearly constant away from them at the value given by Eq. (4.15).

4.6 Dipole superfluids and monopole superfluids

We have shown that magnetic and electric dipole superfluids under a pseudo-magnetic field form vortex lattices with distinctly different electromagnetic field textures. The magnetic-dipole system exhibits a positive feedback effect for the applied field, resulting in discontinuous domain walls that separate neighboring vortices. In contrast, the electric-dipole system shows a negative feedback effect, leading to a strong suppression of the pseudo-magnetic field away from the vortex core. The latter behavior resembles the vortex lattice in type-II superconductors (electric-monopole superfluids), but with a significant difference: the magnetic field in superconductors decays exponentially away from the vortex, whereas the pseudo-magnetic field in electric-dipole superfluids converges to a constant value proportional to $\propto 1/(1+\eta_p)$. In this section, we discuss the origins of these different behaviors among the three distinct classes of systems — superconductors, magnetic-dipole

superfluids, and electric-dipole superfluids — through their key equations.

In the three cases, the superfluid free energy $F_{\rm GL}$ [Eqs. (3.5), (4.4), (2.13)] and the supercurrent [Eqs. (3.7), (4.6), (2.15)] share the same functional form with respect to the corresponding vector potential, i.e., $\mathbf{A}$ for superconductors, and $\mathbf{A}_{\rm m}$ ($\mathbf{A}_p$) for magnetic (electric)-dipole superfluid. Accordingly, the supercurrent and vector potential obey the same relationship. When the phase θ is constant, in particular, we have the London-type equation $\mathbf{j} \propto -\mathbf{A}$, $\mathbf{j}_{\rm m} \propto \mathbf{A}_{\rm m}$, and $\mathbf{j}_{\rm p} \propto -\mathbf{A}_{\rm p}$.

However, a difference lies in the relationship between the vector potential and the real magnetic/electric field:

$$\begin{aligned}
&\boldsymbol{\nabla} \times \mathbf{A} = \mathbf{B} \quad \text{(electric monopole)},\\
&\mathbf{A}_{\rm m} = g_{\rm AC}\mathbf{E} \times \mathbf{e}_z \quad \text{(magnetic dipole)}.\\
&\mathbf{A}_{\rm p} = g_{\rm HMW}\,\mathbf{B} \times \mathbf{e}_z \quad \text{(electric dipole)},
\end{aligned} \tag{4.16}$$

As an inverse effect, the relationship between the supercurrent and the induced magnetization / polarization is also different, as

$$\begin{aligned}
&\boldsymbol{\nabla} \times \mathbf{M} = \mathbf{j} \quad \text{(electric monopole)},\\
&\mathbf{P} = g_{\rm AC}\,\mathbf{j}_{\rm m} \times \mathbf{e}_z \quad \text{(magnetic dipole)},\\
&\mathbf{M} = -g_{\rm HMW}\,\mathbf{j}_{\rm p} \times \mathbf{e}_z \quad \text{(electric dipole)},
\end{aligned} \tag{4.17}$$

Note that Equations (4.16) and (4.17) represent different aspects of the same phenomenon. In fact, Eq. (4.17) can be derived from the variation of the free energy with the same form, under condition of Eq. (4.16).

In Eqs. (4.16) and (4.17), the crucial difference between monopoles and dipoles is in the existence/absence of the spatial derivative $\boldsymbol{\nabla}$. For the monopole case, in particular, these relations with London's equation $\mathbf{j} \propto \mathbf{A}$ lead to $\boldsymbol{\nabla} \times \boldsymbol{\nabla} \times \mathbf{A} \propto \mathbf{A}$ or $\boldsymbol{\nabla}^2\mathbf{B} \propto \mathbf{B}$, resulting in an exponential decay of the magnetic field (Meissner effect). In contrast, in dipole superfluids, the spatial derivative term is absent, resulting in a linear relationship between the external field and the induced field. Consequently, the external fields are amplified or suppressed by a factor of $(1-\eta)^{-1}$ in magnetic-dipole superfluids and $(1+\eta_p)^{-1}$ in electric-dipole superfluids, where the opposite signs in front of η and η_p correspond to positive and negative feedback, respectively.

Finally, the origin of the opposite feedback effects in the magnetic and electric dipole systems is explained as follows. Both systems share the parallel relationships described by Eqs. (4.16) and (4.17), which lead to to the same anti-parallel orientations between the external field $\mathbf{E}_{\rm ext}$ / $\mathbf{B}_{\rm ext}$

and the induced dipole density $\mathbf{P}\,/\,\mathbf{M}$. Here we note that the negative sign in $\mathbf{M}$ in Eq. (4.17) cancels with the negative sign in $\mathbf{j}_{\rm p} \propto -\mathbf{A}_{\rm p}$. However, opposite signs come in the relations between the induced dipole density and the feedback fields: $\mathbf{E}_{\rm int} = -\mathbf{P}/\varepsilon_0$ and $\mathbf{B}_{\rm int} = +\mu_0\mathbf{M}$, resulting in positive and negative feedback, respectively.

Discussion

The domain formation with singular domain walls is a particularly remarkable feature of magnetic-dipole superfluids, with no counterparts in other physical systems. In order to experimentally observe this, we need a magnetic-dipole superfluid satisfying $\eta = g_{\rm AC}^2\Psi_\infty^2/(m^*\varepsilon_0) \gtrsim 1$ [Eq. (3.20)], which requires large spin-orbit coupling, high density of condensate, and small effective mass. We provide a rough estimation of η for a magnon BEC in Yttrium Iron Garnet (YIG), a representative example of currently available materials. In magnetic insulators, $g_{\rm AC}$ is typically 10^6 times as large as in vacuum [47, 48]. The superfluid density can be assumed about $\Psi_\infty^2 \sim 10^{21}$ cm^{-3} [11]. The effective mass is obtained by $m^* = \hbar^2/(2JSa^2)$ by considering ferromagnetic Heisenberg model, where J is the nearest-neighbor ferromagnetic exchange coupling, S is the effective spin and a is the lattice constant. Using material parameters from experiments, we have $J \approx 1.37$ K, $S \approx 14.3$, and $a \approx 12.4$ Å [108, 109]. Under these conditions, we have $\eta \sim 0.36$. We also present an estimation of the magnitude of pseudo-magnetic field. Considering the spatially modulating electric field Eq. (3.4), the dimensionless pseudo-magnetic field is given by $|\tilde{B}_{\rm m}| = g_{\rm AC}\mathcal{E}/(\hbar/\xi^2)$. In the case of YIG, the value $|\tilde{B}_{\rm m}| = 0.02$ used in our calculations corresponds to a reasonable condition with an electric field gradient of $\mathcal{E} = 0.01$ V nm^{-2} and a superfluid coherence length of $\xi = 1$ nm.

Throughout this study, we assumed that the bosons constituting the superfluid have a fixed dipole moment. In the case of magnons, this assumption is justified because magnon creation, as defined by the Holstein-Primakoff transformation, corresponds to a spin-lowering operator, where each magnon is associated with a dipole moment of $g\mu_B$. For excitons as electric dipoles, on the other hand, the dipole moment can change if the relative orbital state of the electron-hole pair is excited (e.g., from $1s$ to $2p$). We assume that the external field is moderate enough to prevent such excitations. Incorporating the variation of the dipole moment would introduce additional nontrivial effects on the properties of dipole superfluids.

We also neglected dipole-dipole interactions between bosons. While this effect is generally considered small in magnon and exciton systems, it is known to give rise to nontrivial phenomena in alkali spinor Bose-Einstein condensates due to the anisotropic nature of dipole-dipole interactions [110]. Investigating its impact on the electromagnetic response is an interesting direction for future work.

Chapter 5

Ferroelectric instability in magnetic-dipole superlfuids

We investigate a ferroelectric instability in a magnon BEC coupled to electric fields via the AC phase. Using a bosonic Bogoliubov-de-Gennes (BdG) mean-field theory, we show that a positive electromagnetic feedback mechanism leads to spontaneous ferroelectric polarization in the absence of an external electric field, when the coupling to the electromagnetic field is strong enough. Specifically, an electric field induces magnon orbital motion via the AC phase, generating an electric polarization that in turn contributes to and enhances the electric field. The resulting polarization breaks spatial inversion symmetry, reshapes the Bogoliubov excitation spectrum, and gives rise to non-reciprocal superfluidity. At the critical point of the phase transition, an exceptional point emerges in a Bogoliubov spectrum, at which not only eigenvalues but also eigenvectors coalesce, and the bosonic quasiparticle and quaihole hybridize to form a single eigenstate that is invariant under the particle–hole transformation. This state can be interpreted as a Majorana boson.

5.1 Review: Bose-Hubbard model in conventional superfluids

In this section, before proceeding to our calculation, we first review the Bogoliubov theory describing the conventional superfluidity of the interacting Bose gas for comparison with the corresponding theory of dipole superfluids. We consider the one-dimensional Bose–Hubbard model, which consists of bosons on a tight-binding lattice with onsite repulsive interaction. The Hamiltonian for this system is expressed as

$$H = -t \sum_i (b_i^\dagger b_{i+1} + b_{i+1}^\dagger b_i) + \frac{U}{2} \sum_i n_i^2, \tag{5.1}$$

where site indices i range from 1 to N, and we impose periodic boundary condition. b_i annihilates a boson and $n_i \equiv b_i^\dagger b_i$ counts the number of bosons in position $x_i = ia$, where a denotes a lattice constant. $t > 0$ denotes a nearest-neighbor hopping amplitude, and $U > 0$ represents the onsite repulsive interaction.

Owing to the discrete translational symmetry of the system, the Bloch wave vector serves as a good quantum number. It is then reasonable to assume that condensation occurs in a lowest-energy single-particle Bloch state [111],

$$\langle b_i \rangle = \sqrt{n_0} e^{ik_c x_i}, \tag{5.2}$$

where n_0 represents the number of condensed bosons per site. The optimal value of $-\pi/a < k_c < \pi/a$ is chosen to minimize the mean-field energy $\langle H \rangle$, giving

$$\langle H \rangle = -2tn_0 \cos k_c a + \frac{U}{2} n_0^2. \tag{5.3}$$

In this case, the lowest-energy single particle state is trivially given by $k_c = 0$. It should be noted that, when the lattice geometry is nontrivial, such as in a kagome lattice, condensation can occur at a finite, nonzero momentum rather than at $k_c = 0$. [112]

We apply the Bogoliubov approximation [111] to examine the excitation properties of the superfluid. To this end, we decompose the bosonic field operator into the Bloch basis as

$$\begin{aligned} b_i &= \langle b_i \rangle + \delta b_i \\ &= \sqrt{n_0} + \frac{1}{\sqrt{N}} \sum_{q \neq 0} e^{iqx_i} \delta b_q, \end{aligned} \tag{5.4}$$

where δb_i corresponds to the fluctuation from the ground-state configuration. By inserting it into the total Hamiltonian $H - \mu N$ and retaining terms up to quadratic order in δb_i, we obtain the bosonic BdG Hamiltonian $H_{\mathrm{BdG}} = 1/2 \sum_{q \neq 0} \psi_q^\dagger H_{\mathrm{B}}(q) \psi_q$, where $\psi_q = (\delta b_q, \delta b_{-q}^\dagger)^t$ denotes the Nambu spinor and

$$H_{\mathrm{B}}(q) = \begin{pmatrix} h(q) & s(q) \\ s^*(-q) & h^*(-q) \end{pmatrix}, \tag{5.5}$$

where

$$\begin{aligned} h(q) &= -2t \cos ka - \mu + 2Un_0 \\ s(q) &= Un_0. \end{aligned} \tag{5.6}$$

The Green's function is defined as $G(q, i\omega) = [i\omega\sigma_z - H_{\mathrm{B}}(q)]^{-1}$, whose poles give the excitation

spectrum. At this stage, the chemical potential μ can be fixed by imposing $\det H_{\rm B}(0) = 0$. This requirement, referred to as the Hugenholtz–Pines relation [111], guarantees a gapless excitation spectrum at $q = 0$. Thus we have

$$\mu = -2t + Un_0 \tag{5.7}$$

Alternatively, the same equation follows from the thermodynamic relation $\mu = \partial \langle H \rangle / \partial n_0$.

We calculate the Bogoliubov energy spectrum by diagonalizing the pseudo-Hermitian matrix [113, 114]

$$\begin{aligned} L(q) &\equiv \sigma_z H_{\rm B}(q), \\ &= \begin{pmatrix} \epsilon_q + Un_0 & Un_0 \\ -Un_0 & -(\epsilon_q + Un_0) \end{pmatrix}, \end{aligned} \tag{5.8}$$

where $\epsilon_q = 2t(1 - \cos q)$. The eigenvalue equations are expressed as

$$L(q) \left|\psi_q^{\pm}\right\rangle = \pm E(\pm q) \left|\psi_q^{\pm}\right\rangle \tag{5.9}$$

where the eigenstates $\left|\psi_q^{\pm}\right\rangle$ represent the quasi-particle and quasi-hole states, respectively.

The energy spectrum is given by

$$\begin{aligned} E(q) &= \sqrt{\epsilon_q(\epsilon_q + 2Un_0)} \\ &\approx \sqrt{\frac{Un_0}{m}}\hbar|q| \quad (|q| \approx 0). \end{aligned} \tag{5.10}$$

We reproduce the typical behaviors of the conventional superfluids well known in the literature [111], which has the gapless linear dispersion around $q = 0$.

5.2 Bose-Hubbard model in magnetic-dipole superfluids

As a minimal theoretical description of a magnon BEC, we consider an annulus-shaped system and adopt the one-dimensional Bose–Hubbard model, which consists of magnons on a tight-binding lattice with onsite repulsive interaction, as illustrated in Fig. 5.1(a). The Hamiltonian for this system is expressed as

$$H_0 = -t \sum_i (e^{-i\theta_{\rm AC}} b_i^\dagger b_{i+1} + e^{+i\theta_{\rm AC}} b_{i+1}^\dagger b_i) + \frac{U}{2} \sum_i n_i^2, \tag{5.11}$$

where site indices i range from 1 to N, and we impose periodic boundary condition. b_i annihilates a magnon and $n_i \equiv b_i^\dagger b_i$ counts the number of magnons in position $x_i = ia$, where a denotes a lattice constant. $t > 0$ denotes a nearest-neighbor hopping amplitude, and $U > 0$ represents the onsite repulsive interaction.

Since magnons have a fixed magnetic dipole moment $\boldsymbol{\mu} = g\mu_B \mathbf{e}_z$, they interact with the electric field $\mathbf{E}$ through the AC phase

$$\theta_{\mathrm{AC}} = -\frac{1}{\hbar}\int \mathbf{A}_{\mathrm{m}} \cdot d\mathbf{r}, \tag{5.12}$$

where

$$\mathbf{A}_{\mathrm{m}} = g_{\mathrm{AC}} \mathbf{E} \times \mathbf{e}_z \tag{5.13}$$

is the effective vector potential. [28] Here, the constant parameter g_{AC} represents the strength of a spin-orbit coupling. In vacuum, it amounts to $g\mu_B/c^2$, however, it greatly enhances about 10^6 times in typical magnetic insulators. [47, 48] A simplified derivation of AC phase can be found in Ref. [115].

The magnon current density $\mathbf{j}_{\mathrm{m}} = j_{i,i+1}/a^2 \ \mathbf{e}_x$ is defined to satisfy the continuity equation

$$\frac{\partial n_i}{\partial t} = \frac{i}{\hbar}[H_0, n_i] \equiv j_{i-1,i} - j_{i,i+1}, \tag{5.14}$$

giving

$$j_{i,i+1} = \frac{it}{\hbar}(e^{i\theta_{\mathrm{AC}}} b_{i+1}^\dagger b_i - e^{-i\theta_{\mathrm{AC}}} b_i^\dagger b_{i+1}). \tag{5.15}$$

This definition agrees with the expression $\mathbf{j}_{\mathrm{m}} = \partial H_0/\partial \mathbf{A}_{\mathrm{m}}$ obtained from the functional derivative of the Hamiltonian with respect to the effective vector potential. Physically, this magnon current is responsible for generating the electric polarization [47–49, 115–117],

$$\mathbf{P} = -\frac{\partial H_0}{\partial \mathbf{E}} = g_{\mathrm{AC}}\ \mathbf{j}_{\mathrm{m}} \times \mathbf{e}_z. \tag{5.16}$$

Through the basic relation $\mathbf{E} = (\mathbf{D} - \mathbf{P})/\epsilon_0$ in electrodynamics, the electric polarization contributes to the total electric field, which in turn produces an additional self-induced AC phase.

Building on these considerations, we seek the total energy of the system, explicitly incorporating the energy of the electromagnetic field. In accordance with the standard prescription, we include the term $\int dV(\mathbf{D}^2 - \mathbf{P}^2)/2\epsilon_0$ as an additional contribution to the original Hamiltonian H_0. [115] Consequently, for the present system, the total Hamiltonian is expressed as

$$H = H_0 - \frac{g_{\mathrm{AC}}^2}{2\epsilon_0 a}\sum_i j_{i,i+1}^2, \tag{5.17}$$

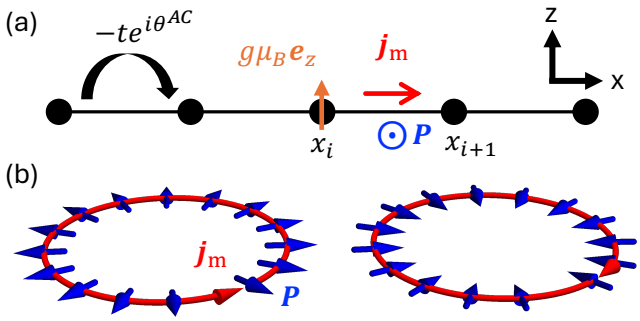


Figure 5.1: Schematic figures of (a) the minimal model of the magnon Bose-Einstein condensate (BEC) with Aharonov-Casher (AC) phase and (b) ferroelectric polarization induced by persistent magnon supercurrent.

where we set $\mathbf{D} = 0$ to examine the intrinsic behavior of the system without the influence of an external electric field.

5.3 Ferroelectricity

Owing to the discrete translational symmetry of the system, the Bloch wave vector serves as a good quantum number. It is then reasonable to assume that condensation occurs in a lowest-energy single-particle Bloch state [111],

$$\langle b_i \rangle = \sqrt{n_0} e^{ik_c x_i}, \tag{5.18}$$

where n_0 represents the number of condensed bosons per site. The optimal value of $-\pi/a < k_c < \pi/a$ is chosen to minimize the mean-field energy $\langle H \rangle$, as described below.

Substituting the ansatz [Eq. (5.18)] into the current operator [Eq. (5.15)] yields the magnon supercurrent $\langle j_{i,i+1} \rangle = (2tn_0/\hbar) \sin \Delta$, where

$$\Delta \equiv k_c a - \theta_{\mathrm{AC}}. \tag{5.19}$$

The magnon supercurrent $\langle \mathbf{j}_{\mathrm{m}} \rangle$ produces the electric polarization by Eq. (5.16), which is an additional electric field. Since we do not apply the external electric field, the AC phase is determined solely from this contribution, giving $\theta_{\mathrm{AC}} = -\eta \sin \Delta$, where

$$\eta = \frac{g_{\mathrm{AC}}^2}{m^* \varepsilon_0 a^3} n_0 \tag{5.20}$$

is the dimensionless parameter [115] that characterizes the strength of the spin-orbit coupling, and $m^* = \hbar^2/(2ta^2)$ is an effective mass for a non-interacting magnon. Thus, Eq. (5.19) can be recast

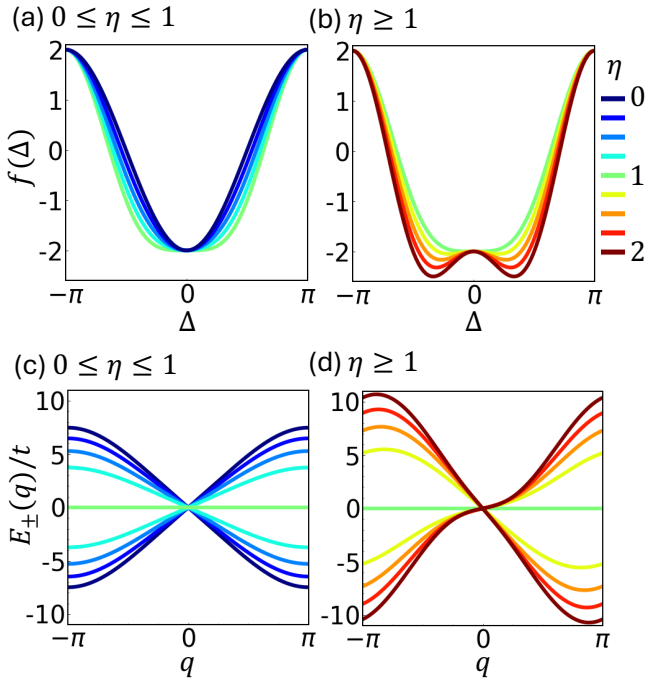


Figure 5.2: (a),(b): The normalized mean-field energy $f(\Delta)$ is shown as a function of Δ, with color representing different values of η. (c),(d): The Bogoliubov spectrum of the bosonic particle $E_+(q) = E(q)$ and hole $E_-(q) = -E(-q)$ are presented, where we set $u = 5$.

as

$$k_c a = \Delta - \eta \sin \Delta, \tag{5.21}$$

thereby fixing the value of k_c for a given Δ.

To identify the lowest-energy single-particle Bloch state, we evaluate the mean-field energy by substituting the ansatz [Eq. (5.18)] into the total Hamiltonian [Eq. (5.17)], giving

$$\langle H \rangle = -2tn_0 \cos \Delta + \frac{U}{2} n_0^2 - t\eta n_0 \sin^2 \Delta, \tag{5.22}$$

that depends on k_c only through Δ. Thus, we begin by minimizing it with respect to Δ, after which we determine the condensate wave vector k_c.

For the sake of clarity, Eq. (5.22) can be simplified to $f(\Delta) = -2\cos\Delta - \eta \sin^2 \Delta$ by neglecting constants and rescaling to a dimensionless form. In Fig. 5.2 (a,b), we plot $f(\Delta)$ with several values of η. Then, Δ that minimizes the mean-field energy is given by

$$\Delta = \begin{cases} 0 & \text{if } 0 \le \eta \le 1, \\ \pm\Delta_0 & \text{if } \eta \ge 1, \end{cases} \tag{5.23}$$

where $\cos \Delta_0 = 1/\eta$ and it satisfies $f'(\pm\Delta_0) = 0$.

When $0 \leq \eta \leq 1$, we observe a minimum of the ground-state energy at $\Delta = 0$, where both the magnon supercurrent and the resulting electric polarization naturally reduce to zero.

When $\eta \geq 1$, the ground-state energy exhibits minima at finite values of Δ, and a persistent magnon supercurrent develops, giving rise to spontaneous electric polarization $P \propto \sin\Delta \neq 0$. This is nothing but ferroelectricity that is accompanied by spontaneous breaking of a space-inversion symmetry. Consequently, the two solutions $\Delta = \pm\Delta_0$ are connected by the parity operation, corresponding to states with opposite directions of electric polarization, as illustrated in Fig. 5.1 (b).

Then, using Δ in Eq. (5.23), we are able to fix the condensate Bloch wave vector

$$k_c a = \begin{cases} 0 & \text{if } 0 \leq \eta \leq 1, \\ \Delta - \eta \sin\Delta & \text{if } \eta \geq 1, \end{cases} \tag{5.24}$$

It is observed that, in the ferroelectric phase, the condensation occurs at a finite wave vector.

In the Appendix of our paper [118], we develop a magnonic analog of Bohr-van Leeuwen theorem: classical magnonic systems in thermal equilibrium are incapable of producing a net electric polarization. This demonstrates that the ferroelectric polarization in magnon BEC presented in this work is attributed to intrinsically quantum mechanical origins.

5.4 Bosonic BdG Hamiltonian

We apply the Bogoliubov approximation [111] to examine the stability and excitation properties of the magnon BEC. The bosonic field operator is decomposed in the Bloch basis as

$$\begin{aligned} b_i &= \langle b_i \rangle + \delta b_i \\ &= \sqrt{n_0} e^{ik_c x_i} + \frac{1}{\sqrt{N}} \sum_{q \neq 0} e^{i(k_c+q)x_i} b_{k_c+q}, \end{aligned} \tag{5.25}$$

where δb_i corresponds to the fluctuation from the ground-state configuration. By inserting Eq. (5.25) into the total Hamiltonian $H - \mu N$ and retaining terms up to quadratic order in δb_i, we obtain the bosonic BdG Hamiltonian $H_{\mathrm{BdG}} = 1/2 \sum_{q \neq 0} \psi_q^\dagger H_{\mathrm{B}}(q) \psi_q$, where $\psi_q = (b_{k_c+q}, b_{k_c-q}^\dagger)^t$ denotes the Nambu spinor and

$$H_{\mathrm{B}}(q) = \begin{pmatrix} h(q) & s(q) \\ s^*(-q) & h^*(-q) \end{pmatrix}, \tag{5.26}$$

where

$$\begin{aligned} h(q) &= -2t\cos(\Delta+q) + 2Un_0 - \mu \\ &\quad - t\eta(1+\cos q - 2\cos(2\Delta+q)), \\ s(q) &= Un_0 - t\eta(\cos q - \cos 2\Delta). \end{aligned} \tag{5.27}$$

The excitation spectrum is given by the poles of the Green's function $G(q, i\omega) = [i\omega\sigma_z - H_{\rm B}(q)]^{-1}$. Since the excitation spectrum must be gapless at $q = 0$ [111], we impose the condition $\det H_{\rm B}(q=0) = 0$, which determines the chemical potential μ as

$$\mu = \begin{cases} -2t + Un_0 & \text{if } 0 \le \eta \le 1, \\ -2t\cos\Delta + Un_0 - 2t\eta\sin^2\Delta & \text{if } \eta \ge 1. \end{cases} \tag{5.28}$$

Alternatively, the same equation can be obtained from the thermodynamic relation $\mu = \partial\langle H\rangle/\partial n_0$, with $\langle H\rangle$ defined in Eq. (5.22), by noting that η depends on n_0 as given in Eq. (5.20).

5.5 Bogoliubov-excitation spectrum

We calculate the Bogoliubov energy spectrum by diagonalizing the non-Hermitian matrix

$$L(q) \equiv \sigma_z H_{\rm B}(q), \tag{5.29}$$

however, it is in fact pseudo-Hermitian $L(q) = \sigma_z L^\dagger(q)\sigma_z$ [113] because $H_{\rm B}(q)$ is a Hermitian matrix. The eigenvalue equations are expressed as

$$L(q)\left|\psi_q^\pm\right\rangle = \pm E(\pm q)\left|\psi_q^\pm\right\rangle \tag{5.30}$$

where the eigenstates $\left|\psi_q^\pm\right\rangle$ represent the quasi-particle and quasi-hole states, respectively. They are related by $\left|\psi_q^-\right\rangle = \sigma_x\left|\psi_{-q}^+\right\rangle^*$ because of the particle-hole symmetry

$$\sigma_x L^*(-q)\sigma_x = -L(q). \tag{5.31}$$

In Fig. (5.2)(c,d), the Bogoliubov band structures are presented, where we set $u \equiv Un_0/t = 5$. The different colors represent various values of η.

When $0 < \eta < 1$ (blue bands), we reproduce the typical behaviors of the conventional superfluids well known in the literature [111], which has the gapless linear dispersion around $q = 0$. Up to this

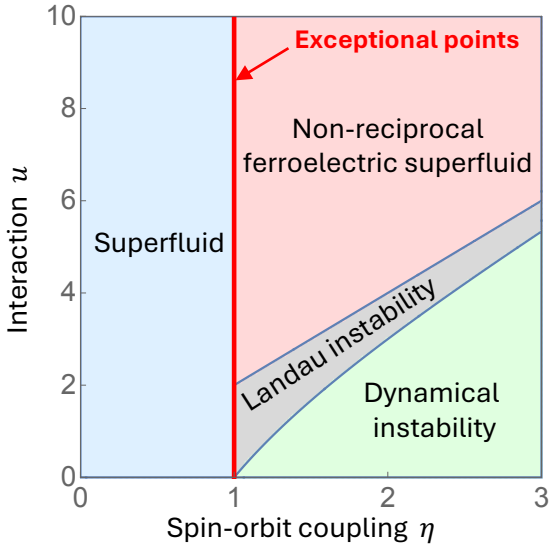


Figure 5.3: The phase diagram in magnon Bose-Einstein condensates. Ferroelectric phase transition occurs at $\eta = 1$, corresponding to exceptional points. The Landau instability occurs at $u = 2\eta$ and the dynamical instability occurs at $u = 2(\eta - 1/\eta)$.

point, the system respects a space-inversion symmetry and satisfies $E(q) = E(-q)$. As η increases from 0 to 1, the particle band and the hole band gradually move closer together.

When $\eta = 1$ (a green band), the particle and hole bands merge into a fully degenerate state with a completely flat dispersion. This is precisely the critical point where the ferroelectric phase transition occurs. Interestingly, this is not a simple degeneracy of eigenvalues, but an exceptional point where the eigenvectors also coalesce. Indeed, the matrix $L(q)$ is given by

$$L(q) \propto \begin{pmatrix} 1 & 1 \\ -1 & -1 \end{pmatrix}, \tag{5.32}$$

that possesses only a single eigenvector $(1, -1)^t$ and is therefore not diagonalizable, corresponding to an exceptional point. Such a property originates from the non-Hermitian nature of the bosonic BdG Hamiltonian. It is also interesting that this zero-energy state can be regarded as a Majorana boson [119–122], because it maps onto itself under the particle–hole transformation.

When $\eta > 1$ (red bands), the particle band and the hole band start to separate again. However, this separation is accompanied by a notable change: the Bogoliubov spectrum becomes non-reciprocal $E(q) \neq E(-q)$. This behavior is naturally understood as a manifestation of a space-inversion symmetry breaking, which originates from the development of spontaneous electric polarization.

5.6 Landau and dynamical instabilities

We have shown that, when $\eta > 1$, the spontaneous magnon supercurrent is induced and the ferroelectricity appears. However, for the ground state to remain stable, the condition $E(q) \geq 0$ must hold for every q. Depending on the relationship between the parameters u and η, the system might exhibit instabilities. This can be seen by focusing on the low-energy ($q \approx 0$) behavior of the energy eigenvalue spectrum

$$E(q) \approx \begin{cases} t\sqrt{2u(1-\eta)}|q| & \text{if } 0 \leq \eta \leq 1, \\ 2t\sqrt{\eta - \frac{1}{\eta}}\left(-\sqrt{\frac{1}{\eta}}q + \sqrt{\frac{u-2(\eta-\frac{1}{\eta})}{2}}|q|\right) & \text{if } \eta \geq 1. \end{cases} \tag{5.33}$$

First, when $0 \leq \eta \leq 1$, the ground state is stable for all $u > 0$. In contrast, when $\eta \geq 1$, the ground state may become unstable. More precisely, as u decreases, $E(q)$ first becomes negative and eventually acquires a complex value.

When $u < 2\eta$, the energy eigenvalue becomes negative, leading to Landau instability [123, 124]. In this regime, creating a quasiparticle lowers the total energy of the system, so the system spontaneously emits excitations. As a result, the superfluid can no longer sustain its flow, and the flow becomes dissipative.

When $u < 2(\eta - 1/\eta)$, the energy eigenvalues become complex, signaling dynamical instability [123, 124]. This is a stronger instability condition than the Landau instability. The imaginary part of the eigenvalue plays the role of a growth or decay rate, resulting in the collapse or fragmentation of the condensate. This condition can also be derived in an alternative manner using the ground-state energy in Eq. (5.22). Since the third term in Eq. (5.22) is proportional to n_0^2 (noting that $\eta \propto n_0$), the expression can be rewritten as $\langle H \rangle = -2tn_0 \cos\Delta + U_{\text{eff}} n_0^2/2$, where

$$U_{\text{eff}} \equiv U - \frac{2t\eta}{n_0}\sin^2\Delta \tag{5.34}$$

represents an effective interaction between bosons. The condition for the dynamical instability coincides with the region where the effective interaction becomes attractive, i.e., $U_{\text{eff}} < 0$.

Under these situations, the mean-field ansatz based on a Bloch wave function [Eq. (5.18)] is no longer valid. A detailed investigation of this regime lies beyond the scope of the present work. Fig. 5.3 presents a phase diagram that summarizes the results of this study.

Chapter 6

Conclusion

In this thesis, we have theoretically investigated electromagnetism in dipole superfluids, especially magnetic-dipole superfluids, represented by magnon Bose-Einstein condensate. We formulated both the phenomenological theory and the microscopic theory, and revealed fundamental electromagnetic properties of magnon BEC which is totally different from those of superconductors.

In Chapter 3 and Chapter 4, we have theoretically studied magnetic and electric dipole superfluids subjected to a pseudo-magnetic field induced by a spatially modulated electromagnetic field. Using a Ginzburg-Landau phenomenological theory that incorporates the geometric AC/HMW phase, we obtained self-consistent solutions by fully accounting for the feedback effect of the electromagnetic field induced by the response current. Under a pseudo-magnetic field, both electric and magnetic dipole superfluids spontaneously form vortex lattices but exhibit distinct field textures. When the electrostatic coupling parameter η exceeds a critical value, magnetic dipole superfluids form a honeycomb lattice with a singular domain wall with diverging pseudo-magnetic fields and polarization charges. This behavior contrasts starkly with conventional superconductors (monopole superfluids). In electric dipole superfluids, the pseudo-magnetic field is concentrated only at vortex cores as in conventional superconductors, but it does not decay exponentially away from the vortices. Despite sharing parallel formulations, magnetic and electric dipole systems exhibit opposite features due to a sign difference in the feedback effect for the applied field. These findings highlight novel field textures and self-organized structures unique to magnetic dipole superfluids, opening new directions in exploring superfluid systems with unconventional electromagnetic responses.

In Chapter 5, beyond the phenomenological theory proposed in Chapter 3, we formulated the microscopic theory and investigated dielectric properties of magnon BEC, that interacts with electric field via geometric AC phase. Through a mean-field analysis, we constructed a phase

diagram as a function of the strength of repulsive interaction u and the spin–orbit coupling η. In particular, when $\eta > 1$, the ferroelectricity appears as a manifestation of the positive feedback loop. We also find that, owing to the spatial-inversion symmetry breaking, the Bogoliubov quasiparticle becomes non-reciprocal. The critical point of the phase transition is characterized by the exceptional point and the Majorana boson, reflecting the non-Hermitian aspect of the underlying bosonic BdG Hamiltonian.

Outlook

As an important future direction concerning ferroelectricity in the magnon BEC, a quantitative comparison between our theoretical predictions and experiments [24] is highly desirable. Although we expect that our minimal model description presented in Chapter 5 captures essential physics, achieving this requires extending the present theory to finite temperatures, as it is currently formulated at absolute zero temperature.

Another future direction is to study quantum geometric phenomena in the magnon BEC, namely the dipole superfluids. In electronic systems, topological superconductivity arising from nontrivial band topology is known to host exotic phenomena such as Majorana fermions and non-Abelian braiding statistics. More recently, quantum geometric quantities, including the quantum metric and quantum geometric tensor, have been recognized as essential ingredients in certain superconductors, such as flat-band superconductors, with direct experimental consequences. Thus, a novel quantum geometric phenomenon is expected to also occur in a magnon BEC, which is an electromagnetic dual of superconductors. Furthermore, due to the distinct mathematical structures between monopoles and dipoles (i.e. AB phase and AC phase), new physics might exist in this system.

In particular, Dirac magnon BEC is a promising direction to study. Analogous to Dirac electrons in graphene, Dirac magnons can emerge in honeycomb magnets. More intriguingly, a quasi-equilibrium Dirac magnon condensate has been theoretically proposed [125], in which condensation occurs at the Dirac point of the magnon band structure. We concentrate on multicomponent effects due to the valley and sublattice degrees of freedom, and quantum geometric effects due to the Berry curvature concentrated at the Dirac points. We investigate the possibility of Berry crvature induced magnon supercurrent, which should give rise to electric polarization. From a broader perspective, the bosonic Bogoliubov–de Gennes system itself is of particular interest. Because bosonic BdG Hamiltonians are intrinsically non-Hermitian, they can host a quantum geometric structure qualitatively distinct from those found in fermionic BdG systems.

Appendix A

General properties of bosonic BdG Hamiltonian

We summarize general properties of the bosonic BdG Hamiltonian

$$H_{\rm BdG} = \frac{1}{2}\sum_{q\neq 0} \psi_q^\dagger H_{\rm B}(q)\psi_q, \tag{A.1}$$

where $\psi_q = (b_q, b_{-q}^\dagger)^t$ denotes the bosonic Nambu spinor and satisfies the bosonic commutation relation $[\psi_q, \psi_q^\dagger] = \sigma_z$. The Bloch Hamiltonian is a $2N \times 2N$ matrix and given by

$$H_{\rm B}(q) = \begin{pmatrix} h(q) & s(q) \\ s^*(-q) & h^*(-q) \end{pmatrix}, \tag{A.2}$$

where $h(q) = h^\dagger(q)$ is a $N \times N$ Hermitian matrix and $s(q)$ is a $N \times N$ matrix that satisfies the relation

$$s(q) = s^t(-q). \tag{A.3}$$

It is different from the fermionic BdG Hamiltonian for superconductors, where the superconducting pair potentials satisfy $\Delta(q) = -\Delta^t(-q)$. Eq. (A.3) is derived as follows.

$$\begin{aligned} \sum_{q\neq 0} s_{\alpha\beta}(q) b_{q\alpha}^\dagger b_{-q\beta}^\dagger &= \sum_{q\neq 0} s_{\alpha\beta}(-q) b_{-q\alpha}^\dagger b_{q\beta}^\dagger \\ &= \sum_{q\neq 0} s_{\alpha\beta}(-q) b_{q\beta}^\dagger b_{-q\alpha}^\dagger \\ &= \sum_{q\neq 0} s_{\beta\alpha}(-q) b_{q\alpha}^\dagger b_{-q\beta}^\dagger. \end{aligned} \tag{A.4}$$

In the first equality, we replace $q \to -q$. In the second equality, we exchange the positions of $b^\dagger_{-q\alpha}$ and $b^\dagger_{q\beta}$ using the bosonic commutation relations. In the third equality, we interchange the indices α and β.

The Bloch Hamiltonian $H_{\rm B}(q)$ is a Hermitian matrix. It is explicitly confirmed as

$$\begin{aligned} H^\dagger_{\rm B}(q) &= \begin{pmatrix} h(q) & s^t(-q) \\ s^\dagger(q) & h^*(-q) \end{pmatrix} \\ &= \begin{pmatrix} h(q) & s(q) \\ s^*(-q) & h^*(-q) \end{pmatrix} \\ &= H_{\rm B}(q), \end{aligned} \tag{A.5}$$

where we used Eq. (A.3).

A.1 Pseudo-Hemiticity

The Green's function is defined as $G(q, i\omega) = [i\omega\sigma_z - H_{\rm B}(q)]^{-1}$, whose poles give the Bogoliubov energy spectrum. Due to the presence of the σ_z in the denominator of the Green's function, the energy spectrum is given by an eigenspectrum of

$$\begin{aligned} L(q) &\equiv \sigma_z H_{\rm B}(q) \\ &= \begin{pmatrix} h(q) & s(q) \\ -s^*(-q) & -h^*(-q) \end{pmatrix}, \end{aligned} \tag{A.6}$$

rather than $H_{\rm B}(q)$ itself. Importantly, $L(q)$ is a non-Hermitian matrix and, in fact, a pseudo-Hermitian matrix

$$\begin{aligned} L^\sharp(q) &\equiv \sigma_z L^\dagger(q) \sigma_z \\ &= L(q), \end{aligned} \tag{A.7}$$

where we used the Hemiticity of $H_{\rm B}(q)$.

A.2 Particle-hole symmetry

Since the matrix is non-Hermitian, it possesses both right eigenvectors

$$L(q)\left|\psi_n^+(q)\right\rangle = E_n(q)\left|\psi_n^+(q)\right\rangle \tag{A.8}$$

$$L(q)\left|\psi_n^-(q)\right\rangle = -E_n(-q)\left|\psi_n^-(q)\right\rangle \tag{A.9}$$

and left eigenvectors

$$\langle\langle\psi_n^+(q)|L(q) = E_n(q)\langle\langle\psi_n^+(q)| \tag{A.10}$$

$$\langle\langle\psi_n^-(q)|L(q) = -E_n(-q)\langle\langle\psi_n^-(q)| \tag{A.11}$$

where the $\pm$ represent the particle and hole states, respectively. $n = 1, 2, 3, ..., N$ represent band indices. They are related by $|\psi_n^-(q)\rangle = \sigma_x |\psi_n^+(-q)\rangle^*$ via the particle-hole symmetry

$$\begin{aligned}\sigma_x L^*(-q)\sigma_x &= \sigma_x \begin{pmatrix} h^*(-q) & s^*(-q) \\ -s(q) & -h(q) \end{pmatrix}\sigma_x \\ &= -L(q).\end{aligned} \tag{A.12}$$

A.3 Diagonalization by para-unitary matrix

To diagonalize the pseudo-Hermitian matrix, we employ the following transformation to the bosonic Nambu spinors

$$\psi_q \to \psi'_q = P^{-1}(q)\psi_q. \tag{A.13}$$

The transformation matrix must preserve the bosonic commutation relations. Therefore, this requirement leads to the condition

$$\begin{aligned}\left[\psi_{q\alpha}, \psi^\dagger_{q\beta}\right] &= \left[P_{\alpha\gamma}(q)\psi'_{q\gamma}, P^*_{\beta\delta}(q)\psi'^\dagger_{q\delta}\right] \\ &= P_{\alpha\gamma}(q)P^*_{\beta\delta}(q)\left[\psi'_{q\gamma}, \psi'^\dagger_{q\delta}\right] \\ &= P_{\alpha\gamma}(q)P^*_{\beta\delta}(q)(\sigma_z)_{\gamma\delta} \\ &= \left(P(q)\sigma_z P^\dagger(q)\right)_{\alpha\beta} \\ &= (\sigma_z)_{\alpha\beta}.\end{aligned} \tag{A.14}$$

Thus, we obtain a para-unitary condition

$$P^{-1}(q) = \sigma_z P^\dagger(q)\sigma_z \equiv P^\sharp(q). \tag{A.15}$$

Using this para-unitary transformation, we have

$$P^{-1}(q)L(q)P(q) = \begin{pmatrix} E(q) & 0 \\ 0 & -E(-q) \end{pmatrix}. \tag{A.16}$$

Finally, the bosonic BdG Hamiltonian is diagonalized as

$$\begin{aligned} H_{\mathrm{BdG}} &= \frac{1}{2}\sum_{q\neq 0} \psi_q^\dagger H_{\mathrm{B}}(q)\psi_q \\ &= \frac{1}{2}\sum_{q\neq 0} (P^{-1}(q)\psi_q)^\dagger P^\dagger(q) H_{\mathrm{B}}(q) P(q)(P^{-1}(q)\psi_q) \\ &= \frac{1}{2}\sum_{q\neq 0} \psi_q'^\dagger \sigma_z P^{-1}(q) L(q) P(q) \psi_q' \\ &= \frac{1}{2}\sum_{q\neq 0} \psi_q'^\dagger \sigma_z \begin{pmatrix} E(q) & 0 \\ 0 & -E(-q) \end{pmatrix} \psi_q'. \end{aligned} \tag{A.17}$$

A.4 Two-band model

We consider the two-band model as the simplest pseudo-Hermitian system. The most general 2×2 pseudo-Hermitian matrix can be expressed as

$$\begin{aligned} L(q) &= \begin{pmatrix} d_0(q)+d_1(q) & d_2(q)-id_3(q) \\ -d_2(q)-id_3(q) & d_0(q)-d_1(q) \end{pmatrix} \\ &= d_0(q)\mathbf{1} + \sum_{\mu=1}^{3} d^\mu(q) K_\mu, \end{aligned} \tag{A.18}$$

where $d_0(q), d_1(q), d_2(q), d_3(q) \in \mathbb{R}$ and

$$\mathbf{1} = \begin{pmatrix} 1 & 0 \\ 0 & 1 \end{pmatrix},\ K_1 = \sigma_z = \begin{pmatrix} 1 & 0 \\ 0 & -1 \end{pmatrix},\ K_2 = i\sigma_y = \begin{pmatrix} 0 & 1 \\ -1 & 0 \end{pmatrix},\ K_3 = -i\sigma_x = \begin{pmatrix} 0 & -i \\ -i & 0 \end{pmatrix}. \tag{A.19}$$

This is analogous to the fact that a general 2×2 Hermitian matrix can be expanded in terms of the Pauli matrices. It is straightforward to obtain the eigenenergy as

$$\begin{aligned} E_{\pm}(q) &= d_0(q) \pm \sqrt{d_1(q)^2 - d_2(q)^2 - d_3(q)^2} \\ &= d_0(q) \pm \|\mathbf{d}(q)\|_{\mathrm{L}}, \end{aligned} \tag{A.20}$$

where $\|\mathbf{d}(q)\|_{\mathrm{L}}$ is a Lorentzian norm. Thus, when $\|\mathbf{d}(q)\|_{\mathrm{L}} > 0$, the parameter space of $\hat{\mathbf{d}}(q) = \mathbf{d}(q)/\|\mathbf{d}(q)\|_{\mathrm{L}}$ becomes a hyperbolic surface (i.e. $x^2 - y^2 - z^2 = 1$) that is identical to the Minkowski spacetime in special relativity. It is totally different from the Hermitian counterpart; when the 2×2 Hermitian matrix is expanded by Pauli matrices, the parameter space becomes a sphere (i.e. $x^2 + y^2 + z^2 = 1$).

Appendix B

Thermodynamic free energy

We present the derivation of the Helmholtz free energy of magnetic dipole superfluids [Eq. (3.12)], and the Gibbs free energy of electric dipole superfluids [Eq. (4.10)], paralleling the argument for the conventional superconductors.

B.1 Magnetic-dipole superfluids

We consider a quasi-static, isothermal process where the external electric field, or $\mathbf{D}(\mathbf{r})$, is slowly introduced to the magnetic-dipole superfluid with the temperature fixed. Here, we consider a general situation where the external electric field $\mathbf{D}$ (and consequently $\mathbf{E}$ and $\mathbf{P}$) depends on position, to account for the system under the pseudo-magnetic field, which needs spatially dependent electric field [Eq. (3.3)]. We assume that the system is at the thermal equilibrium of given $\mathbf{D}(\mathbf{r})$ and T at every moment of the process. As in a general dielectric material, the change in the Helmholtz free energy from the initial state (i) with $\mathbf{D} = 0$ to the finial state (f) with $\mathbf{D} = \mathbf{D}(\mathbf{r})$ is written as

$$\begin{aligned} F[\mathbf{D}(\mathbf{r}), T] - F[0, T] &= \int_{\mathrm{i}}^{\mathrm{f}} \int d\mathbf{r}\ \mathbf{E}(\mathbf{r}) \cdot \delta\mathbf{D}(\mathbf{r}) \\ &= \int_{\mathrm{i}}^{\mathrm{f}} \int d\mathbf{r} \left(\frac{\mathbf{D} \cdot \delta\mathbf{D} - \mathbf{P} \cdot \delta\mathbf{P}}{\varepsilon_0} - \mathbf{P} \cdot \delta\mathbf{E} \right) \\ &= \int d\mathbf{r}\ \frac{\mathbf{D}^2 - \mathbf{P}^2}{2\varepsilon_0} - \int_{\mathrm{i}}^{\mathrm{f}} \int d\mathbf{r}\ \mathbf{P} \cdot \delta\mathbf{E} \end{aligned} \tag{B.1}$$

Here $\int_{\mathrm{i}}^{\mathrm{f}} \cdots \delta\mathbf{D}(\mathbf{r})$ represents the functional integral in $\mathbf{D}(\mathbf{r})$.

The last term in Eq. (B.1) coincides with the change of GL energy functional $F_{\mathrm{GL}}[\Psi, \mathbf{A}_{\mathrm{m}}]$,

because the infinitesimal change in $F_{\rm GL}$ in the process is written as

$$\begin{aligned}\delta F_{\rm GL}[\Psi, \mathbf{A}_{\rm m}] &= \int d\mathbf{r} \frac{\delta F_{\rm GL}}{\delta \mathbf{A}_{\rm m}} \cdot \delta \mathbf{A}_{\rm m} \\ &= \int d\mathbf{r}\ \mathbf{j}_{\rm m} \cdot \delta \mathbf{A}_{\rm m} \\ &= \int d\mathbf{r}\ \mathbf{j}_{\rm m} \cdot (g_{\rm AC}\ \delta \mathbf{E} \times \mathbf{e}_z) \\ &= -\int d\mathbf{r}\ (g_{\rm AC}\ \mathbf{j}_{\rm m} \times \mathbf{e}_z) \cdot \delta \mathbf{E} \\ &= -\int d\mathbf{r}\ \mathbf{P} \cdot \delta \mathbf{E}, \end{aligned} \tag{B.2}$$

where we used Eqs. (3.2), (3.7) and (3.8). Here we note that the variation $\delta F_{\rm GL}$ should also include $\delta F_{\rm GL}/\delta\Psi$ and $\delta F_{\rm GL}/\delta\Psi^*$, while these terms just vanish because we assume that the GL equation Eq. (3.6) holds throughout the quasi-static process. From Eq. (B.1) and Eq. (B.2), we obtain Eq. (3.12).

We can readily check that the self-consistent equations are derived by the variation of the total Helmholtz free energy with $\mathbf{D}$ fixed. Eq. (3.6) is given by $\delta F/\delta\Psi = 0$, since $\delta F/\delta\Psi = \delta F_{\rm GL}/\delta\Psi$. Eq. (3.10) is obtained by $\delta F/\delta \mathbf{A}_{\rm m} = 0$, noting

$$\begin{aligned}\frac{\delta F}{\delta \mathbf{A}_{\rm m}} &= \frac{\delta F_{\rm GL}}{\delta \mathbf{A}_{\rm m}} + \frac{\delta}{\delta \mathbf{A}_{\rm m}} \left(\frac{\mathbf{D}^2 - \mathbf{P}^2}{2\varepsilon_0} \right) \\ &= \mathbf{j}_{\rm m} + \frac{\varepsilon_0}{g_{\rm AC}^2} (\mathbf{A}_{\rm m}^{\rm ext} - \mathbf{A}_{\rm m}) = 0, \end{aligned} \tag{B.3}$$

where we used relations $\mathbf{P} = \mathbf{D} - \varepsilon_0 \mathbf{E}$ and $\mathbf{E} = g_{\rm AC}^{-1}(\mathbf{e}_z \times \mathbf{A}_{\rm m}) + E_z \mathbf{e}_z$.

B.2 Electric-dipole superfluids

We derive the expression of the Gibbs free energy $G[\mathbf{H}, T]$, Eq. (4.10). We consider a quasi-static, isothermal process where the external magnetic field $\mathbf{H}$ is slowly introduced to the electric-dipole superfluid with temperature fixed. The change in the Gibbs free energy from the initial state (i) with $\mathbf{H} = 0$ to the final state (f) with $\mathbf{H}$ is given by

$$\begin{aligned} G[\mathbf{H}(\mathbf{r}), T] - G[0, T] &= -\int_{\rm i}^{\rm f} \int d\mathbf{r}\ \mathbf{B}(\mathbf{r}) \cdot \delta \mathbf{H}(\mathbf{r}) \\ &= \int_{\rm i}^{\rm f} \int d\mathbf{r} \left(\frac{\mathbf{B} \cdot \delta \mathbf{B}}{\mu_0} - \mathbf{H} \cdot \delta \mathbf{B} - \mathbf{B} \cdot \delta \mathbf{H} - \mathbf{M} \cdot \delta \mathbf{B} \right) \\ &= \int d\mathbf{r} \left(\frac{\mathbf{B}^2}{2\mu_0} - \mathbf{B} \cdot \mathbf{H} \right) - \int_{\rm i}^{\rm f} \int d\mathbf{r}\ \mathbf{M} \cdot \delta \mathbf{B} \end{aligned} \tag{B.4}$$

We can show that the last term in Eq. (B.4) coincides with the change in $F_{\rm GL}$ by the following argument. In a quasi-static process, the infinitesimal change in the GL free energy functional is given by

$$\begin{aligned}
\delta F_{\rm GL}[\Psi, \mathbf{A}_{\rm p}] &= \int d\mathbf{r} \frac{\delta F_{\rm GL}}{\delta \mathbf{A}_{\rm p}} \cdot \delta \mathbf{A}_{\rm p} \\
&= -\int d\mathbf{r}\ \mathbf{j}_{\rm p} \cdot \delta \mathbf{A}_{\rm p} \\
&= -\int d\mathbf{r}\ \mathbf{j}_{\rm p} \cdot (g_{\rm HMW}\ \delta \mathbf{B} \times \mathbf{e}_z) \\
&= \int d\mathbf{r}\ (g_{\rm HMW}\ \mathbf{j}_{\rm p} \times \mathbf{e}_z) \cdot \delta \mathbf{B} \\
&= -\int \mathbf{M} \cdot \delta \mathbf{B}, \qquad \text{(B.5)}
\end{aligned}$$

where we used Eq. (4.6), and we noted that $\delta F_{\rm GL}/\delta\Psi = \delta F_{\rm GL}/\delta\Psi^* = 0$ throughout the process. Equations (B.4) and (B.5) lead to the Eq. (4.10).

We check that self-consistent equations are derived by the variation of the total Gibbs free energy while fixing $\mathbf{H}$. Eq. (4.5) is straightforwardly derived from $\delta G/\delta\Psi = 0$ since $\delta G/\delta\Psi = \delta F_{\rm GL}/\delta\Psi$. Eq. (4.9) is obtained by $\delta G/\delta \mathbf{A}_{\rm p} = 0$, noting

$$\begin{aligned}
\frac{\delta G}{\delta \mathbf{A}_{\rm p}} &= \frac{\delta F_{\rm GL}}{\delta \mathbf{A}_{\rm p}} + \frac{\delta}{\delta \mathbf{A}_{\rm p}} \left(\frac{\mathbf{B}^2}{2\mu_0} - \mathbf{B} \cdot \mathbf{H} \right) \\
&= -\mathbf{j}_{\rm p} + \frac{1}{\mu_0 p^2} (\mathbf{A}_{\rm p} - \mathbf{A}_{\rm p}^{\rm ext}) \\
&= 0, \qquad \text{(B.6)}
\end{aligned}$$

where we used relations $\mathbf{B} = \mu_0(\mathbf{H} + \mathbf{M})$ and $\mathbf{B} = g_{\rm HMW}^{-1}(\mathbf{e}_z \times \mathbf{A}_{\rm p}) + B_z \mathbf{e}_z$.

Acknowledgments

I would like to express my deepest gratitude to my supervisor, Prof. Mikito Koshino, for his continuous guidance, encouragement, and invaluable advice throughout the course of my doctoral research. His attitude toward research and his dedication to producing high-quality work have had a profound influence on my scientific career. I am also sincerely grateful to Prof. Takuto Kawakami for devoting substantial time to discussions that ranged from the overall direction of my research to concrete technical problems I encountered. His thoughtful advice and patient guidance were invaluable at every stage of this work. I am sincerely grateful to the members of my thesis committee, Prof. Masayuki Ochi, Prof. Hajime Yoshino, and Prof. Tetsuya Onogi, for their careful reading of this dissertation and for providing insightful comments and constructive suggestions that significantly improved the quality of this work. I am thankful to Prof. Hidenori Fukaya and Dr. Naoto Kan for our fruitful collaboration, through which we wrote a paper that exemplifies a successful interdisciplinary exchange between condensed-matter physics and high-energy physics. This collaboration broadened my scientific perspective and resulted in a highly rewarding research outcome. I would also like to acknowledge the members of Koshino Group, especially Dr. Tenta Tani and Dr. Takaaki Joya, with whom I challenged the Ph.D. program together. Their mutual encouragement, discussions, and shared struggles made my doctoral course both stimulating and enjoyable. I am grateful to the secretariat Mari Homma and Yuki Harada for their continuous support, which greatly facilitated my doctoral research. This work was financially supported by JSPS KAKENHI Grant No.JP23KJ1518, which I gratefully acknowledge. Finally, I would like to express my heartfelt appreciation to my parents Hidenori Yamamoto and Harue Yamamoto for their understanding, encouragement, and unwavering support, which allowed me to pursue and complete my Ph.D.

Bibliography

[1] A. Ikeda, Y. H. Matsuda, K. Sato, Y. Ishii, H. Sawabe, D. Nakamura, S. Takeyama, and J. Nasu, Nature Communications **14**, 1744 (2023), ISSN 2041-1723, URL https://doi.org/10.1038/s41467-023-37125-4.

[2] Z. Jiang, W. Lou, Y. Liu, Y. Li, H. Song, K. Chang, W. Duan, and S. Zhang, Phys. Rev. Lett. **124**, 166401 (2020), URL https://link.aps.org/doi/10.1103/PhysRevLett.124.166401.

[3] Q.-f. Sun and X. C. Xie, Phys. Rev. B **87**, 245427 (2013), URL https://link.aps.org/doi/10.1103/PhysRevB.87.245427.

[4] H. Yang, J. Zeng, Y. Shao, Y. Xu, X. Dai, and X.-Z. Li, Phys. Rev. B **109**, 075167 (2024), URL https://link.aps.org/doi/10.1103/PhysRevB.109.075167.

[5] H. Nishida, S. Miyakoshi, T. Kaneko, K. Sugimoto, and Y. Ohta, Phys. Rev. B **99**, 035119 (2019), URL https://link.aps.org/doi/10.1103/PhysRevB.99.035119.

[6] R. Wang, O. Erten, B. Wang, and D. Y. Xing, Nature Communications **10**, 210 (2019), ISSN 2041-1723, URL https://doi.org/10.1038/s41467-018-08203-9.

[7] H. Liu, H. Jiang, X. C. Xie, and Q.-f. Sun, Phys. Rev. B **86**, 085441 (2012), URL https://link.aps.org/doi/10.1103/PhysRevB.86.085441.

[8] G. Sethi, Y. Zhou, L. Zhu, L. Yang, and F. Liu, Phys. Rev. Lett. **126**, 196403 (2021), URL https://link.aps.org/doi/10.1103/PhysRevLett.126.196403.

[9] G. Sethi, M. Cuma, and F. Liu, Phys. Rev. Lett. **130**, 186401 (2023), URL https://link.aps.org/doi/10.1103/PhysRevLett.130.186401.

[10] H. Wei, S.-P. Chao, and V. Aji, Phys. Rev. Lett. **109**, 196403 (2012), URL https://link.aps.org/doi/10.1103/PhysRevLett.109.196403.

[11] S. O. Demokritov, V. E. Demidov, O. Dzyapko, G. A. Melkov, A. A. Serga, B. Hillebrands, and A. N. Slavin, Nature **443**, 430 (2006), ISSN 1476-4687, URL https://doi.org/10.1038/nature05117.

[12] D. A. Bozhko, A. A. Serga, P. Clausen, V. I. Vasyuchka, F. Heussner, G. A. Melkov, A. Pomyalov, V. S. L'vov, and B. Hillebrands, Nature Physics **12**, 1057 (2016), ISSN 1745-2481, URL https://doi.org/10.1038/nphys3838.

[13] D. A. Bozhko, A. J. E. Kreil, H. Y. Musiienko-Shmarova, A. A. Serga, A. Pomyalov, V. S. L'vov, and B. Hillebrands, Nature Communications **10**, 2460 (2019), ISSN 2041-1723, URL https://doi.org/10.1038/s41467-019-10118-y.

[14] K. S. Olsson, K. An, G. A. Fiete, J. Zhou, L. Shi, and X. Li, Phys. Rev. X **10**, 021029 (2020), URL https://link.aps.org/doi/10.1103/PhysRevX.10.021029.

[15] B. Divinskiy, H. Merbouche, V. E. Demidov, K. O. Nikolaev, L. Soumah, D. Gouéré, R. Lebrun, V. Cros, J. B. Youssef, P. Bortolotti, et al., Nature Communications **12**, 6541 (2021), ISSN 2041-1723, URL https://doi.org/10.1038/s41467-021-26790-y.

[16] T. Nikuni, M. Oshikawa, A. Oosawa, and H. Tanaka, Phys. Rev. Lett. **84**, 5868 (2000), URL https://link.aps.org/doi/10.1103/PhysRevLett.84.5868.

[17] C. Rüegg, N. Cavadini, A. Furrer, H.-U. Güdel, K. Krämer, H. Mutka, A. Wildes, K. Habicht, and P. Vorderwisch, Nature **423**, 62 (2003), ISSN 1476-4687, URL https://doi.org/10.1038/nature01617.

[18] T. Giamarchi, C. Rüegg, and O. Tchernyshyov, Nature Physics **4**, 198 (2008), ISSN 1745-2481, URL https://doi.org/10.1038/nphys893.

[19] A. A. Aczel, Y. Kohama, C. Marcenat, F. Weickert, M. Jaime, O. E. Ayala-Valenzuela, R. D. McDonald, S. D. Selesnic, H. A. Dabkowska, and G. M. Luke, Phys. Rev. Lett. **103**, 207203 (2009), URL https://link.aps.org/doi/10.1103/PhysRevLett.103.207203.

[20] E. Sonin, Advances in Physics **59**, 181 (2010), https://doi.org/10.1080/00018731003739943, URL https://doi.org/10.1080/00018731003739943.

[21] V. Zapf, M. Jaime, and C. D. Batista, Rev. Mod. Phys. **86**, 563 (2014), URL https://link.aps.org/doi/10.1103/RevModPhys.86.563.

[22] W. Yuan, Q. Zhu, T. Su, Y. Yao, W. Xing, Y. Chen, Y. Ma, X. Lin, J. Shi, R. Shindou, et al., Science Advances **4**, eaat1098 (2018), https://www.science.org/doi/pdf/10.1126/sciadv.aat1098, URL https://www.science.org/doi/abs/10.1126/sciadv.aat1098.

[23] N. Esaki, Y. Akagi, and H. Katsura, Phys. Rev. Res. **6**, L032050 (2024), URL https://link.aps.org/doi/10.1103/PhysRevResearch.6.L032050.

[24] S. Kimura, K. Kakihata, Y. Sawada, K. Watanabe, M. Matsumoto, M. Hagiwara, and H. Tanaka, Nature Communications **7**, 12822 (2016), ISSN 2041-1723, URL https://doi.org/10.1038/ncomms12822.

[25] S. Kimura, K. Kakihata, Y. Sawada, K. Watanabe, M. Matsumoto, M. Hagiwara, and H. Tanaka, Phys. Rev. B **95**, 184420 (2017), URL https://link.aps.org/doi/10.1103/PhysRevB.95.184420.

[26] S. Kimura, M. Matsumoto, and H. Tanaka, Phys. Rev. Lett. **124**, 217401 (2020), URL https://link.aps.org/doi/10.1103/PhysRevLett.124.217401.

[27] K. Sakurai, S. Kimura, S. Awaji, M. Matsumoto, and H. Tanaka, Phys. Rev. B **102**, 064104 (2020), URL https://link.aps.org/doi/10.1103/PhysRevB.102.064104.

[28] Y. Aharonov and A. Casher, Phys. Rev. Lett. **53**, 319 (1984), URL https://link.aps.org/doi/10.1103/PhysRevLett.53.319.

[29] F. Meier and D. Loss, Phys. Rev. Lett. **90**, 167204 (2003), URL https://link.aps.org/doi/10.1103/PhysRevLett.90.167204.

[30] K. Nakata, S. K. Kim, J. Klinovaja, and D. Loss, Phys. Rev. B **96**, 224414 (2017), URL https://link.aps.org/doi/10.1103/PhysRevB.96.224414.

[31] K. Nakata, J. Klinovaja, and D. Loss, Phys. Rev. B **95**, 125429 (2017), URL https://link.aps.org/doi/10.1103/PhysRevB.95.125429.

[32] Y. Wang, Z.-G. Zhu, and G. Su, Phys. Rev. B **110**, 054434 (2024), URL https://link.aps.org/doi/10.1103/PhysRevB.110.054434.

[33] Y. Su and X. R. Wang, Phys. Rev. B **96**, 104437 (2017), URL https://link.aps.org/doi/10.1103/PhysRevB.96.104437.

[34] A. Wagh and V. Rakhecha, Progress in Particle and Nuclear Physics **37**, 485 (1996), ISSN 0146-6410, URL https://www.sciencedirect.com/science/article/pii/0146641096000567.

[35] K. Sangster, E. A. Hinds, S. M. Barnett, E. Riis, and A. G. Sinclair, Phys. Rev. A **51**, 1776 (1995), URL https://link.aps.org/doi/10.1103/PhysRevA.51.1776.

[36] Y. Avishai, K. Totsuka, and N. Nagaosa, Journal of the Physical Society of Japan **88**, 084705 (2019), https://doi.org/10.7566/JPSJ.88.084705, URL https://doi.org/10.7566/JPSJ.88.084705.

[37] Y. Avishai and Y. B. Band, *Aharonov–bohm and aharonov–casher effects in meso-scopic physics: A brief review* (2023), 2302.06300.

[38] M. König, A. Tschetschetkin, E. M. Hankiewicz, J. Sinova, V. Hock, V. Daumer, M. Schäfer, C. R. Becker, H. Buhmann, and L. W. Molenkamp, Phys. Rev. Lett. **96**, 076804 (2006), URL https://link.aps.org/doi/10.1103/PhysRevLett.96.076804.

[39] R. I. Shekhter, O. Entin-Wohlman, M. Jonson, and A. Aharony, Phys. Rev. Lett. **129**, 037704 (2022), URL https://link.aps.org/doi/10.1103/PhysRevLett.129.037704.

[40] Y. Yamane, S. Fukami, and J. Ieda, Phys. Rev. Lett. **128**, 147201 (2022), URL https://link.aps.org/doi/10.1103/PhysRevLett.128.147201.

[41] A. V. Balatsky and B. L. Altshuler, Phys. Rev. Lett. **70**, 1678 (1993), URL https://link.aps.org/doi/10.1103/PhysRevLett.70.1678.

[42] E. Grosfeld and A. Stern, Proceedings of the National Academy of Sciences **108**, 11810 (2011), https://www.pnas.org/doi/pdf/10.1073/pnas.1101469108, URL https://www.pnas.org/doi/abs/10.1073/pnas.1101469108.

[43] W. J. Elion, J. J. Wachters, L. L. Sohn, and J. E. Mooij, Phys. Rev. Lett. **71**, 2311 (1993), URL https://link.aps.org/doi/10.1103/PhysRevLett.71.2311.

[44] S. S. Seidov and M. V. Fistul, Phys. Rev. A **103**, 062410 (2021), URL https://link.aps.org/doi/10.1103/PhysRevA.103.062410.

[45] X. Zhang, T. Liu, M. E. Flatté, and H. X. Tang, Phys. Rev. Lett. **113**, 037202 (2014), URL https://link.aps.org/doi/10.1103/PhysRevLett.113.037202.

[46] R. O. Serha, V. I. Vasyuchka, A. A. Serga, and B. Hillebrands, Phys. Rev. B **108**, L220404 (2023), URL https://link.aps.org/doi/10.1103/PhysRevB.108.L220404.

[47] H. Katsura, N. Nagaosa, and A. V. Balatsky, Phys. Rev. Lett. **95**, 057205 (2005), URL https://link.aps.org/doi/10.1103/PhysRevLett.95.057205.

[48] T. Liu and G. Vignale, Phys. Rev. Lett. **106**, 247203 (2011), URL https://link.aps.org/doi/10.1103/PhysRevLett.106.247203.

[49] G. Go, D. An, H.-W. Lee, and S. K. Kim, Nano Letters **24**, 5968 (2024), ISSN 1530-6984, URL https://doi.org/10.1021/acs.nanolett.4c00430.

[50] J. E. Hirsch, Phys. Rev. B **60**, 14787 (1999), URL https://link.aps.org/doi/10.1103/PhysRevB.60.14787.

[51] Q.-f. Sun, H. Guo, and J. Wang, Phys. Rev. B **69**, 054409 (2004), URL https://link.aps.org/doi/10.1103/PhysRevB.69.054409.

[52] Y. Tokura, S. Seki, and N. Nagaosa, Reports on Progress in Physics **77**, 076501 (2014), URL https://dx.doi.org/10.1088/0034-4885/77/7/076501.

[53] I. Solovyev, R. Ono, and S. Nikolaev, Phys. Rev. Lett. **127**, 187601 (2021), URL https://link.aps.org/doi/10.1103/PhysRevLett.127.187601.

[54] Y. Zhu, E. Kleinherbers, L. Levitov, and Y. Tserkovnyak, Phys. Rev. B **112**, L100405 (2025), URL https://link.aps.org/doi/10.1103/j8rt-c6qp.

[55] P. Bruno and V. K. Dugaev, Phys. Rev. B **72**, 241302 (2005), URL https://link.aps.org/doi/10.1103/PhysRevB.72.241302.

[56] W. Chen and M. Sigrist, Phys. Rev. B **89**, 024511 (2014), URL https://link.aps.org/doi/10.1103/PhysRevB.89.024511.

[57] K. Nakata, K. A. van Hoogdalem, P. Simon, and D. Loss, Phys. Rev. B **90**, 144419 (2014), URL https://link.aps.org/doi/10.1103/PhysRevB.90.144419.

[58] K. Nakata, Phys. Rev. B **104**, 104402 (2021), URL https://link.aps.org/doi/10.1103/PhysRevB.104.104402.

[59] Y. Wu, H. Jiang, H. Chen, H. Liu, J. Liu, and X. C. Xie, Phys. Rev. Lett. **128**, 106804 (2022), URL https://link.aps.org/doi/10.1103/PhysRevLett.128.106804.

[60] Z.-b. Wang, Q.-f. Sun, and X. C. Xie, The European Physical Journal B **86**, 496 (2013), ISSN 1434-6036, URL https://doi.org/10.1140/epjb/e2013-40798-2.

[61] Z.-q. Bao, X. C. Xie, and Q.-f. Sun, Nature Communications **4**, 2951 (2013), ISSN 2041-1723, URL https://doi.org/10.1038/ncomms3951.

[62] Q.-f. Sun, Z.-t. Jiang, Y. Yu, and X. C. Xie, Phys. Rev. B **84**, 214501 (2011), URL https://link.aps.org/doi/10.1103/PhysRevB.84.214501.

[63] D. Jérome, T. M. Rice, and W. Kohn, Phys. Rev. **158**, 462 (1967), URL https://link.aps.org/doi/10.1103/PhysRev.158.462.

[64] W. Kohn, Phys. Rev. Lett. **19**, 439 (1967), URL https://link.aps.org/doi/10.1103/PhysRevLett.19.439.

[65] L. V. Butov, A. Zrenner, G. Abstreiter, G. Böhm, and G. Weimann, Phys. Rev. Lett. **73**, 304 (1994), URL https://link.aps.org/doi/10.1103/PhysRevLett.73.304.

[66] D. V. Khveshchenko, Phys. Rev. Lett. **87**, 246802 (2001), URL https://link.aps.org/doi/10.1103/PhysRevLett.87.246802.

[67] J. P. Eisenstein and A. H. MacDonald, Nature **432**, 691 (2004), ISSN 1476-4687, URL https://doi.org/10.1038/nature03081.

[68] H. Cercellier, C. Monney, F. Clerc, C. Battaglia, L. Despont, M. G. Garnier, H. Beck, P. Aebi, L. Patthey, H. Berger, et al., Phys. Rev. Lett. **99**, 146403 (2007), URL https://link.aps.org/doi/10.1103/PhysRevLett.99.146403.

[69] H. Min, R. Bistritzer, J.-J. Su, and A. H. MacDonald, Phys. Rev. B **78**, 121401 (2008), URL https://link.aps.org/doi/10.1103/PhysRevB.78.121401.

[70] A. Kogar, M. S. Rak, S. Vig, A. A. Husain, F. Flicker, Y. I. Joe, L. Venema, G. J. MacDougall, T. C. Chiang, E. Fradkin, et al., Science **358**, 1314 (2017), https://www.science.org/doi/pdf/10.1126/science.aam6432, URL https://www.science.org/doi/abs/10.1126/science.aam6432.

[71] J. I. A. Li, T. Taniguchi, K. Watanabe, J. Hone, and C. R. Dean, Nature Physics **13**, 751 (2017), ISSN 1745-2481, URL https://doi.org/10.1038/nphys4140.

[72] Z. Wang, D. A. Rhodes, K. Watanabe, T. Taniguchi, J. C. Hone, J. Shan, and K. F. Mak, Nature **574**, 76 (2019), ISSN 1476-4687, URL https://doi.org/10.1038/s41586-019-1591-7.

[73] L. A. Jauregui, A. Y. Joe, K. Pistunova, D. S. Wild, A. A. High, Y. Zhou, G. Scuri, K. D. Greve, A. Sushko, C.-H. Yu, et al., Science **366**, 870 (2019), https://www.science.org/doi/pdf/10.1126/science.aaw4194, URL https://www.science.org/doi/abs/10.1126/science.aaw4194.

[74] L. Ma, P. X. Nguyen, Z. Wang, Y. Zeng, K. Watanabe, T. Taniguchi, A. H. MacDonald, K. F. Mak, and J. Shan, Nature **598**, 585 (2021), ISSN 1476-4687, URL https://doi.org/10.1038/s41586-021-03947-9.

[75] J. Huang, B. Jiang, J. Yao, D. Yan, X. Lei, J. Gao, Z. Guo, F. Jin, Y. Li, Z. Yuan, et al., Phys. Rev. X **14**, 011046 (2024), URL https://link.aps.org/doi/10.1103/PhysRevX.14.011046.

[76] A. V. Balatsky, Y. N. Joglekar, and P. B. Littlewood, Phys. Rev. Lett. **93**, 266801 (2004), URL https://link.aps.org/doi/10.1103/PhysRevLett.93.266801.

[77] O. Dubinkin, J. May-Mann, and T. L. Hughes, Phys. Rev. B **103**, 125129 (2021), URL https://link.aps.org/doi/10.1103/PhysRevB.103.125129.

[78] Q.-D. Jiang, Z.-q. Bao, Q.-F. Sun, and X. C. Xie, Scientific Reports **5**, 11925 (2015), ISSN 2045-2322, URL https://doi.org/10.1038/srep11925.

[79] X.-G. He and B. H. J. McKellar, Phys. Rev. A **47**, 3424 (1993), URL https://link.aps.org/doi/10.1103/PhysRevA.47.3424.

[80] M. Wilkens, Phys. Rev. Lett. **72**, 5 (1994), URL https://link.aps.org/doi/10.1103/PhysRevLett.72.5.

[81] I. V. Borisenko, B. Divinskiy, V. E. Demidov, G. Li, T. Nattermann, V. L. Pokrovsky, and S. O. Demokritov, Nature Communications **11**, 1691 (2020), ISSN 2041-1723, URL https://doi.org/10.1038/s41467-020-15468-6.

[82] M. Schneider, T. Brächer, D. Breitbach, V. Lauer, P. Pirro, D. A. Bozhko, H. Y. Musiienko-Shmarova, B. Heinz, Q. Wang, T. Meyer, et al., Nature Nanotechnology **15**, 457 (2020), ISSN 1748-3395, URL https://doi.org/10.1038/s41565-020-0671-z.

[83] A. J. E. Kreil, H. Y. Musiienko-Shmarova, P. Frey, A. Pomyalov, V. S. L'vov, G. A. Melkov, A. A. Serga, and B. Hillebrands, Phys. Rev. B **104**, 144414 (2021), URL https://link.aps.org/doi/10.1103/PhysRevB.104.144414.

[84] S. Hayashida, L. Huberich, D. Flavián, Z. Yan, K. Y. Povarov, S. Gvasaliya, and A. Zheludev, Phys. Rev. Res. **3**, 033053 (2021), URL https://link.aps.org/doi/10.1103/PhysRevResearch.3.033053.

[85] D. Flavián, P. A. Volkov, S. Hayashida, K. Y. Povarov, S. Gvasaliya, P. Chandra, and A. Zheludev, Phys. Rev. Lett. **130**, 216501 (2023), URL https://link.aps.org/doi/10.1103/PhysRevLett.130.216501.

[86] K. Nakata, P. Simon, and D. Loss, Phys. Rev. B **92**, 134425 (2015), URL https://link.aps.org/doi/10.1103/PhysRevB.92.134425.

[87] S. Owerre, Annals of Physics **399**, 93 (2018), ISSN 0003-4916, URL https://www.sciencedirect.com/science/article/pii/S0003491618302677.

[88] S. A. Owerre, Scientific Reports **8**, 4431 (2018), ISSN 2045-2322, URL https://doi.org/10.1038/s41598-018-22779-8.

[89] B. Li and A. A. Kovalev, Phys. Rev. Lett. **125**, 257201 (2020), URL https://link.aps.org/doi/10.1103/PhysRevLett.125.257201.

[90] V. N. Krivoruchko and A. S. Savchenko, Phys. Rev. B **109**, 184437 (2024), URL https://link.aps.org/doi/10.1103/PhysRevB.109.184437.

[91] Y. Wang, Z.-G. Zhu, and G. Su, Phys. Rev. B **110**, 054434 (2024), URL https://link.aps.org/doi/10.1103/PhysRevB.110.054434.

[92] Z. Jin, Z. Zeng, Y. Cao, and P. Yan, Phys. Rev. Lett. **133**, 196701 (2024), URL https://link.aps.org/doi/10.1103/PhysRevLett.133.196701.

[93] O. O. Boliasova and V. N. Krivoruchko, Phys. Rev. B **111**, 174440 (2025), URL https://link.aps.org/doi/10.1103/PhysRevB.111.174440.

[94] Y. Wang, Z.-G. Zhu, and G. Su, Phys. Rev. B **111**, 165150 (2025), URL https://link.aps.org/doi/10.1103/PhysRevB.111.165150.

[95] S. Birnkammer, M. Knap, J. Knolle, A. Mook, and A. Bastianello, Phys. Rev. B **112**, 094417 (2025), URL https://link.aps.org/doi/10.1103/btt2-mp62.

[96] Q.-H. Chen, F.-J. Huang, Y.-P. Fu, and H. Su, Phys. Rev. B **111**, 064426 (2025), URL https://link.aps.org/doi/10.1103/PhysRevB.111.064426.

[97] T. Yokoyama and Y. Tada, Phys. Rev. B **111**, 064415 (2025), URL https://link.aps.org/doi/10.1103/PhysRevB.111.064415.

[98] J.-C. Li and A. Du, *Quantum controlling and the topological properties of the magnon photo-transport in two-dimensional collinear ferromagnet* (2025), 2504.06852, URL https://arxiv.org/abs/2504.06852.

[99] H. Wei, R. Han, and X. Wei, Phys. Rev. Lett. **75**, 2071 (1995), URL https://link.aps.org/doi/10.1103/PhysRevLett.75.2071.

[100] J. P. Dowling, C. P. Williams, and J. D. Franson, Phys. Rev. Lett. **83**, 2486 (1999), URL https://link.aps.org/doi/10.1103/PhysRevLett.83.2486.

[101] S. Lepoutre, A. Gauguet, G. Trénec, M. Büchner, and J. Vigué, Phys. Rev. Lett. **109**, 120404 (2012), URL https://link.aps.org/doi/10.1103/PhysRevLett.109.120404.

[102] W. Chen, P. Horsch, and D. Manske, Phys. Rev. B **87**, 214502 (2013), URL https://link.aps.org/doi/10.1103/PhysRevB.87.214502.

[103] A. A. Wood, B. H. J. McKellar, and A. M. Martin, Phys. Rev. Lett. **116**, 250403 (2016), URL https://link.aps.org/doi/10.1103/PhysRevLett.116.250403.

[104] M. Tinkham, *Introduction to Superconductivity* (Dover, 1996).

[105] M. Stone and R. Roy, Phys. Rev. B **69**, 184511 (2004), URL https://link.aps.org/doi/10.1103/PhysRevB.69.184511.

[106] N. R. Cooper, N. K. Wilkin, and J. M. F. Gunn, Phys. Rev. Lett. **87**, 120405 (2001), URL https://link.aps.org/doi/10.1103/PhysRevLett.87.120405.

[107] D. Doshi and A. Gromov, Communications Physics **4**, 44 (2021), ISSN 2399-3650, URL https://doi.org/10.1038/s42005-021-00540-4.

[108] M. A. Gilleo and S. Geller, Phys. Rev. **110**, 73 (1958), URL https://link.aps.org/doi/10.1103/PhysRev.110.73.

[109] I. S. Tupitsyn, P. C. E. Stamp, and A. L. Burin, Phys. Rev. Lett. **100**, 257202 (2008), URL https://link.aps.org/doi/10.1103/PhysRevLett.100.257202.

[110] T. Lahaye, C. Menotti, L. Santos, M. Lewenstein, and T. Pfau, Reports on Progress in Physics **72**, 126401 (2009), URL https://dx.doi.org/10.1088/0034-4885/72/12/126401.

[111] H. Shi and A. Griffin, Physics Reports **304**, 1 (1998), ISSN 0370-1573, URL https://www.sciencedirect.com/science/article/pii/S0370157398000155.

[112] Y.-Z. You, Z. Chen, X.-Q. Sun, and H. Zhai, Phys. Rev. Lett. **109**, 265302 (2012), URL https://link.aps.org/doi/10.1103/PhysRevLett.109.265302.

[113] Y. Ashida, Z. Gong, and M. Ueda, Advances in Physics **69**, 249 (2020), https://doi.org/10.1080/00018732.2021.1876991, URL https://doi.org/10.1080/00018732.2021.1876991.

[114] K. Kawabata, K. Shiozaki, M. Ueda, and M. Sato, Phys. Rev. X **9**, 041015 (2019), URL https://link.aps.org/doi/10.1103/PhysRevX.9.041015.

[115] K. Yamamoto, T. Kawakami, and M. Koshino, Communications Physics **8**, 171 (2025), ISSN 2399-3650, URL https://doi.org/10.1038/s42005-025-02088-z.

[116] D. Q. To, F. Garcia-Gaitan, Y. Ren, J. M. O. Zide, M. B. Jungfleisch, J. Q. Xiao, B. K. Nikolić, G. W. Bryant, and M. F. Doty, Proceedings of the National Academy of Sciences **122**, e2507255122 (2025), https://www.pnas.org/doi/pdf/10.1073/pnas.2507255122, URL https://www.pnas.org/doi/abs/10.1073/pnas.2507255122.

[117] J. Tang and R. Cheng, *Proper theory of magnon orbital angular momentum* (2025), 2510.03322, URL https://arxiv.org/abs/2510.03322.

[118] K. Yamamoto, T. Kawakami, and M. Koshino, *Ferroelectricity in magnon bose-einstein condensate: non-reciprocal superfluidity, exceptional points and majorana bosons* (2025), 2512.22073, URL https://arxiv.org/abs/2512.22073.

[119] Q.-R. Xu, V. P. Flynn, A. Alase, E. Cobanera, L. Viola, and G. Ortiz, Phys. Rev. B **102**, 125127 (2020), URL https://link.aps.org/doi/10.1103/PhysRevB.102.125127.

[120] V. P. Flynn, E. Cobanera, and L. Viola, Phys. Rev. Lett. **127**, 245701 (2021), URL https://link.aps.org/doi/10.1103/PhysRevLett.127.245701.

[121] V. P. Flynn, E. Cobanera, and L. Viola, Phys. Rev. B **108**, 214312 (2023), URL https://link.aps.org/doi/10.1103/PhysRevB.108.214312.

[122] N. Okuma, Phys. Rev. B **110**, 014516 (2024), URL https://link.aps.org/doi/10.1103/PhysRevB.110.014516.

[123] B. Wu and Q. Niu, Phys. Rev. A **64**, 061603 (2001), URL https://link.aps.org/doi/10.1103/PhysRevA.64.061603.

[124] B. Wu and Q. Niu, New Journal of Physics **5**, 104 (2003), URL https://doi.org/10.1088/1367-2630/5/1/104.

[125] P. O. Sukhachov, S. Banerjee, and A. V. Balatsky, Phys. Rev. Res. **3**, 013002 (2021), URL https://link.aps.org/doi/10.1103/PhysRevResearch.3.013002.